

## Where is the Detection Limit?

### Investigation of the LAND/R<sup>3</sup>B-setup Detection Efficiency using Monte Carlo Simulations

BACHELOR THESIS IN ENGINEERING PHYSICS

*Authors:*

Mattias Eliasson  
Anders Furufors  
Linnea Johansson  
Thomas Lundqvist  
Jens Roderus

*Supervisors:*

Andreas Heinz  
Håkan Johansson  
Ronja Thies

## Abstract

This report investigates the detection efficiency of the experimental setup LAND/R<sup>3</sup>B. This is done through Monte Carlo simulations. The simulation software GEANT4, via the wrapper program GGLAND, is used with the reconstruction tool LAND/R<sup>3</sup>B-TRACKER.

Beams of different isotopes of carbon, boron and beryllium, produced by reactions of parent isotopes <sup>16</sup>C, <sup>17</sup>C and <sup>18</sup>C, were simulated passing through the setup. The LAND/R<sup>3</sup>B-TRACKER reconstructs the nuclear masses and momentum 4-vectors of the ions from the data acquired by the detectors. The efficiency is determined assuming the nuclear masses follow a normal distribution. Events that fell inside the distribution were considered correctly reconstructed. The detection efficiency is the quotient of the correctly reconstructed events and the total number of simulated events.

It was found that this efficiency depends on several variables, where the geometry of the detectors is one. The detector GFI2 (Großer FIBerdetektor 2) was found to be the detector that has the lowest acceptance. The addition of transverse momentum to the ions was also found to affect the efficiency.

## Sammanfattning

Den här rapporten undersöker detektionseffektiviteten hos experimentuppställningen LAND/ R<sup>3</sup>B. Detta görs med hjälp av Monte Carlo-simuleringar. Simuleringsmjukvaran GEANT4, via wrapper-programmet GGLAND, används tillsammans med rekonstruktionsverktyget LAND/R<sup>3</sup>B-TRACKER.

Strålar av olika isotoper av kol, bor och beryllium, producerade i reaktioner av moderisotoper <sup>16</sup>C, <sup>17</sup>C och <sup>18</sup>C, simuleras passera genom uppställningen. LAND/R<sup>3</sup>B-TRACKER rekonstruerar jonernas massor från simulerad data. Effektiviteten bestäms genom att anta att massorna är normalfördelade. Händelser som följer fördelningen anses vara korrekt rekonstruerade. Detektionseffektiviteten är kvoten av de korrekt rekonstruerade händelserna och det totala antalet simulerade händelser.

Det fastställs att effektiviteten beror på flera variabler, där geometrin för detektorerna är en. Detektorn GFI2 (Großer FIBerdetektor 2) är den detektor som har lägst acceptans. Tillägg av transversell rörelsemängd till jonerna påverkar också effektiviteten.

# Acknowledgements

We would like to express our gratitude towards our supervisors who have helped us make this project not only successful, but also enjoyable. We want to thank Andreas Heinz who has been an excellent teacher and of great help. We also want to thank Ronja Thies for always answering our countless questions and providing us with everything needed for the project. We are thankful for the advice and support from Håkan Johansson regarding simulations and other computer related issues. Lastly, we would like to thank Simon Lindberg for helping out with the LAND/R<sup>3</sup>B-TRACKER.

The Authors, Gothenburg, May 2016

# Contents

<b>1</b>	<b>Introduction</b>	<b>1</b>
1.1	Statement of the Problem . . . . .	1
1.2	Scope . . . . .	2
1.3	Outline of the Report . . . . .	3
<b>2</b>	<b>Background</b>	<b>4</b>
2.1	The LAND/R <sup>3</sup> B Setup . . . . .	4
2.1.1	Production of Unstable Nuclei . . . . .	4
2.1.2	Experimental Setup at Cave C . . . . .	5
2.2	Three Detectors of Special Interest . . . . .	7
2.2.1	Silicon Strip Detectors, SST . . . . .	7
2.2.2	Großer Fiberdetektors, GFI . . . . .	8
2.2.3	Time of Flight Wall, TFW . . . . .	8
2.3	Reconstruction of the Ions . . . . .	8
2.4	Consequences of the Collisions . . . . .	10
2.5	Half-lives of the Ions . . . . .	11
<b>3</b>	<b>Simulations</b>	<b>12</b>
3.1	Software Tools . . . . .	12
3.1.1	GEANT4 . . . . .	12
3.1.2	GGLAND . . . . .	13
3.1.3	LAND/R <sup>3</sup> B-TRACKER . . . . .	13
3.1.4	ROOT . . . . .	13
3.2	Elimination of Paddle Spacing in TFW . . . . .	14
3.3	Deriving a Realistic Kick . . . . .	14
3.4	Simulation Method . . . . .	15
3.5	Data Analysis . . . . .	16
<b>4</b>	<b>Results</b>	<b>17</b>
4.1	Carbon Fragments . . . . .	17
4.2	Boron Fragments . . . . .	18
4.3	Beryllium Fragments . . . . .	19
<b>5</b>	<b>Discussion</b>	<b>21</b>
5.1	Limiting Detectors . . . . .	21
5.2	Maximum Efficiency . . . . .	21
5.3	Limitations of the Tracker . . . . .	22
5.4	General Effects of Transversal Momentum . . . . .	23
5.5	Missing the GFI2-detector . . . . .	24
5.6	Increasing Efficiency with Kick . . . . .	25
5.7	Dependency of A/Z on Beam Direction . . . . .	26
5.8	Poor Fits in ROOT . . . . .	27
<b>6</b>	<b>Conclusion</b>	<b>28</b>

<b>7</b>	<b>Glossary</b>	<b>29</b>
<b>A</b>	<b>Tables of Efficiencies</b>	<b>i</b>
A.1	Reaction Products from a Beam of $^{16}\text{C}$ . . . . .	i
A.2	Reaction Products from a Beam of $^{17}\text{C}$ . . . . .	ii
A.3	Reaction Products from a Beam of $^{18}\text{C}$ . . . . .	iii
<b>B</b>	<b>Derivation of the Formula for the Magnetic Rigidity</b>	<b>iv</b>
<b>C</b>	<b>Positions of the Detectors in the Simulations</b>	<b>v</b>
<b>D</b>	<b>C++ Function for Calculating Efficiencies</b>	<b>vi</b>
<b>E</b>	<b>Example of a GGLAND-script</b>	<b>vii</b>
<b>F</b>	<b>Förkortad version på svenska</b>	<b>viii</b>
F.1	Inledning . . . . .	viii
F.2	Bakgrund . . . . .	ix
F.2.1	LAND/R <sup>3</sup> B-uppställningen och S393-experimentet . . . . .	ix
F.2.2	Introduktion av de tre mest relevanta detektorerna . . . . .	x
F.2.3	Rekonstruktion av jonerna . . . . .	x
F.2.4	Resultat av kollisionerna . . . . .	xi
F.3	Simuleringar . . . . .	xi
F.3.1	Mjukvara . . . . .	xi
F.3.2	Realistisk rekyl . . . . .	xii
F.3.3	Simuleringsmetod och dataanalys . . . . .	xii
F.4	Resultat . . . . .	xiii
F.5	Diskussion . . . . .	xv
F.5.1	Begränsande detektorer och maximal effektivitet . . . . .	xvi
F.5.2	Den maximala effektiviteten . . . . .	xvi
F.5.3	Påverkan av rekyl . . . . .	xvi
F.6	Slutsats . . . . .	xvii

# List of abbreviations

This is a list of abbreviations that are used in this thesis.

Abbreviation	Meaning	Short description
ALADiN	A Large Acceptance Dipole magnet	Large magnet at LAND/R <sup>3</sup> B
GSI	Gesellschaft für Schwerionenforschung	Accelerator Laboratory in Germany
UNILAC	UNIversal Linear ACcelerator	Linear particle accelerator at GSI
SIS18	SchwerIonenSynchrotron 18	Synchrotron at GSI
FRS	FRagment Separator	Fragment Separator at GSI
POS	POStion detector	Detector in LAND/R <sup>3</sup> B
ROLU	Rechts, Oben, Links, Unten	Beam adjuster in LAND/R <sup>3</sup> B
PSP	Position Sensitive Pin diode	Detector in LAND/R <sup>3</sup> B
XB	Crystal Ball	Detector in LAND/R <sup>3</sup> B
LAND	Large Area Neutron Detector	Detector in LAND/R <sup>3</sup> B
PDC	Proton Drift Chamber	Detector in LAND/R <sup>3</sup> B
DTF	Dicke Time of Flight Wall	Detector in LAND/R <sup>3</sup> B
SST	Silicon Strip detector	Detector in LAND/R <sup>3</sup> B
GFI	Großer Fliberdetektor	Detector in LAND/R <sup>3</sup> B
TFW	Time of Flight Wall	Detector in LAND/R <sup>3</sup> B
ZM	Zero Momentum (frame)	An inertial frame

# List of notation

This is a list of symbols that are used in this thesis.

Symbol	Definition
$A$	Mass number
$Z$	Atomic number
$q$	Charge
$\Delta E$	Energy loss
$m$	Mass
$\vec{F}$	Force vector
$\vec{p}$	Momentum vector
$c$	Speed of light, 299 792 458 m/s
$\tau$	Proper time
$t$	Time
$\vec{v}$	Velocity vector
$\beta$	The quotient $v/c$
$\gamma$	Lorentz factor, $\frac{1}{\sqrt{1-\beta^2}}$
$\rho$	Bending radius
$\vec{E}$	Electric field vector
$\vec{B}$	Magnetic field vector
$B\rho$	Magnetic rigidity
$\sigma$	Standard deviation
$\mu$	Mean value

# 1 Introduction

The very lightest of the chemical elements came into existence a very short time after the universe was born. Later, matter accumulated to create stars where nuclei heavier than beryllium were able to form for the very first time. The nuclear reactions that happen in stars and supernovae are responsible for all but the lightest elements. The goal to understand the processes behind these nuclear reactions is perhaps the most fundamental reason to study nuclear physics.

In the quest for unraveling fundamental principles of nature, nuclear reactions are studied using various accelerators worldwide. Nuclear reactions are also studied for technological and medical purposes. For practical reasons, highly radioactive nuclei are not as well understood as stable isotopes. Only since the 1980s ion beam facilities exist, able to create radioactive ions. Many of the nuclear physics experiments performed today therefore focus in particular on studying unstable nuclei.

In 2010, an experiment on neutron-rich nuclei (the S393-experiment) was carried out at the GSI Helmholtz Centre for Heavy Ion Research, in Darmstadt, Germany that focused on light unstable nuclei. It was performed making use of an experimental setup (the LAND/R<sup>3</sup>B-setup) optimized for kinematically complete measurements using relativistic radioactive beams. In order to analyze the results obtained by the LAND/R<sup>3</sup>B-setup, as from any experiment, it is important to know what the limitations of the detectors are, i.e. under what conditions the detectors fail to detect the reaction products. One point of interest is to determine how many of the fragments miss the detectors or are lost on the way through the experimental setup. It is also interesting to know the fraction of incorrectly reconstructed events. Given that information it is possible to understand what processes can be measured.

## 1.1 Statement of the Problem

The aim of this project is to find the detection limit of the LAND/R<sup>3</sup>B-setup. The setup has been used in several experiments, among them the S393-experiment, and will be used in future experiments as well. The detection limit will be found using the simulation tool GEANT4 together with GGLAND as well as the analysis tool LAND/R<sup>3</sup>B-TRACKER. The results of this project will be shared with those involved in the S393-experiment and be of value in the ongoing analysis of the experimental data as well as in other future and past experiments using the LAND/R<sup>3</sup>B-setup.

The limitations of the experiment will be examined primarily in two ways. One of

the questions is to what extent increased transverse momentum of the beam affects the efficiency. The efficiency is defined as correctly reconstructed events divided by total amount of simulated events<sup>1</sup>. The transverse momentum of a fragment caused by a reaction in a setup like that of the S393-experiment affects its path through the experimental setup and therefore influences its detection efficiency. By examining this, the corresponding effect will be identifiable in the experimental data of the S393-experiment. Similarly, it is useful to learn how different isotopes have different acceptances. The second point to be examined is therefore to what degree different isotopes are transmitted through the full length of the experimental setup and reconstructed correctly.

As mentioned above, the simulation tools used for this project will be GEANT4 along with LAND/R<sup>3</sup>B-TRACKER. Using these particular tools in the project is an important part of the task, because the same software is used in analyzing the results of the LAND/R<sup>3</sup>B-experiments. In order to eliminate potential deviations caused by a difference in reconstruction tools this project must use the same software as the experiments do.

## 1.2 Scope

The project uses simulations. That allows for example, a clear definition of incoming particles and detector resolutions in the LAND/R<sup>3</sup>B-setup and therefore allow us to compare results under various conditions in order to isolate parameters of interest. The limitations of the project are essentially the limitations of the simulation toolkit used, GEANT4. GEANT4 is specifically designed for simulating nuclear and particle physics, and takes into account a vast number of physical processes and possible outcomes. Therefore the simulations will very closely resemble what may happen experimentally, thus making the limitations of our simulations few in that aspect.

The project investigates what parameters affect the efficiency of detection in the LAND/R<sup>3</sup>B-setup, focusing on the effect of transverse momentum of the fragments. Simulations were done for various fragments, limited to reaction products from beams of carbon isotopes <sup>16</sup>C, <sup>17</sup>C and <sup>18</sup>C. These potentially react to form other carbon isotopes, isotopes of boron or isotopes of beryllium. Simulations were done down to <sup>9</sup>C, <sup>8</sup>B and <sup>7</sup>Be. The simulations were done without added momentum as well as with 400 MeV/c added, one, two and three times, in isotropically random directions for each case. The motivation behind the choice of these values will be discussed in Chapter 3. The simulations were done with 300 000 simulated events each, a value which has been found to be sufficient for this project. Simulations with larger number of entries would require more time without reducing the statistical uncertainties of the simulations significantly. With more time at hand this project could have been extended to deal with different magnetic fields and isotopes or with other effects on the detection efficiency, like the resolution of the detectors.

---

<sup>1</sup>In this report, reconstructing means the process of determining the mass number and 4-momentum vector from the data enquired by the detectors.

## 1.3 Outline of the Report

This report is aimed to provide a full understanding of the project and all its aspects. That will be done by giving the reader an understanding of the theory behind the LAND/R<sup>3</sup>B-setup as well as the physics that will be dealt with. This is described in Chapter 2. In Chapter 3, the reader will learn about the practical aspects of the project, while Chapter 4 and 5 present the results and discuss them.

## 2 Background

In this chapter some necessary theoretical knowledge is presented. In order to find the limiting conditions of the LAND/R<sup>3</sup>B-experiments, it is important to have an understanding of the experimental setup as well as of the nature of the isotopes that are studied. The first two sections (Section 2.1 and Section 2.2) focus on the setup of the LAND/R<sup>3</sup>B-experiments as well as on three types of detectors that are of particular interest to this project. These detectors are the Silicon STrip detectors (SST), the Großer FIBerdetektors (GFI) and the Time of Flight Wall (TFW). From the measured quantities in the S393-experiment all necessary information about the outgoing particles can be extracted. The necessary relations to do that are presented and explained in detail in Section 2.3. The last two sections (Section 2.4 and Section 2.5) introduce the physical processes that can occur in experiments like the S393-experiment and, hence, are of interest for the analysis of the results.

### 2.1 The LAND/R<sup>3</sup>B Setup

The particular experimental setup on which this project is based is the LAND/R<sup>3</sup>B-setup at the GSI Helmholtz Centre for Heavy Ion Research in Darmstadt, Germany. The results of this project are relevant for past and future experiments at this experimental setup. One experiment that used this setup was the S393-experiment carried out in 2010. The S393-experiment focused on neutron-rich nuclei of atomic number 4 to 10 (that is in the region beryllium to neon). As can be read in the experiment proposal [1], one of the goals of the experiment is to gain a better understanding of the reaction rates in astrophysical environments of reactions important for r-process nucleosynthesis (that is the creation of heavy elements). This is done by studying the results of electromagnetic excitation of the heavy ions in the setup. The second interest of the experiment is to study the structure of nuclei near the driplines, i.e. to understand the nuclear formations heavier or as heavy as possible in bound states. That was done through knocking out nucleons in those isotopes, from inner as well as from outer nuclear single-particle orbitals, by collision with a target material. The experimental setup that was used is described in detail in the following sections.

#### 2.1.1 Production of Unstable Nuclei

The S393-experiment studies unstable nuclei with half-lives in the order down to milliseconds. In order to use such unstable ions they must be produced on site. The production of unstable nuclei and selection of the nuclei of interest is done using the UNiversal Linear ACcelerator (UNILAC), the SchwerIonenSynchrotron 18 (SIS18) and the FRagment Separator (FRS).

In the UNILAC, ions can be accelerated to up to 20 percent of the speed of light [2]. For further acceleration the ions are injected into the synchrotron accelerator SIS18 in which they can reach velocities as high as 90 percent of the speed of light [3]. After the acceleration process, the ions collide with a relatively light target. In the case of the S393-experiment a beam of  $^{40}\text{Ar}$  at an energy of 490 MeV per nucleon collided with a target of  $^9\text{Be}$  upon which the ions of  $^{40}\text{Ar}$  were fragmented. Fragments with various masses and energies were produced in the collision depending on the impact parameter with the target nuclei [4].

In order to select the isotopes of interest from all the reaction products, the fragment beam is guided through the FRS [5]. The FRS separates the fragments in terms of magnetic rigidity through the use of several magnets in a way that is described by Equation 2 in Section 2.3. It is therefore selecting fragments according to their mass over charge ratio as they have approximately the same velocity. In order to select the fragments in terms of both mass and charge separately, the fragments pass through a degrader in which they lose energy proportional to the square of their charge, as can be seen in Equation 3 in Section 2.3. By sending the fragments through yet another setup of magnets, a beam of fragments of a particular mass and charge can be selected. This method is used for producing beams for the LAND/R<sup>3</sup>B-setup and as a result only a few species of nuclei reach the setup [4].

### 2.1.2 Experimental Setup at Cave C

The LAND/R<sup>3</sup>B-setup is located at Cave C. This is the area which the ions enter after having been produced and separated, yielding a beam consisting of a particular set of isotopes [5]. In the LAND/R<sup>3</sup>B-setup the beam collides with a stationary target. This target can be made of, for example, carbon, lead or plastic, all serving different experimental purposes. The reaction products are identified through the use of a magnet, A Large Acceptance DIpole magNet (ALADiN), and detectors of different types. The picture below, Figure 1, shows the LAND/R<sup>3</sup>B-setup. The incoming beam direction is illustrated with a large arrow.

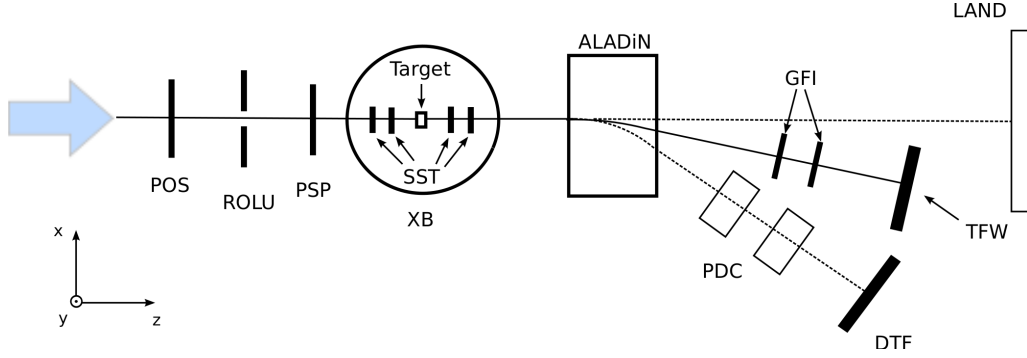


Figure 1: Schematic illustration of the LAND/R<sup>3</sup>B-setup, as it was used in the S393-experiment. An incoming beam of ions is impinging on the target. At collision with the target nuclei some of the projectile nuclei are fragmented. The reaction products are detected and separated into the fragment, neutron and proton arms. These arms end in the TFW, LAND and DTF detectors respectively.

After entering the LAND/R<sup>3</sup>B-setup the beam passes through the POSition (POS) detector, the Rechts-Oben-Links-Unten (ROLU) and the Position Sensitive Pin diode (PSP), as can be seen in Figure 1. The POS-detector detects time of the incoming ions [4]. The task of ROLU is to eliminate all ions from further analysis that are not close enough to the central beam trajectory. The focusing is done by using sets of strategically placed quadrupole magnets. The PSP is used for charge identification. After passing POS, ROLU and PSP, the ion beam approaches the target. The target in the R<sup>3</sup>B/LAND-setup is placed at the center of a shell-like detector called Crystal Ball (XB), illustrated in Figure 1. Collisions with the nuclei in the target result in some cases in a removal of one or more neutrons or protons from the incoming ions. The resulting excitation may also result in the emission of photons or further nucleons. The XB-detector detects the protons, neutrons and gamma photons that are not ejected in the beam direction. In addition to that there are eight SST-detectors inside the XB. Two SST-detectors before and two after the target provide position and energy loss data of the beam and of reaction products. The other four detectors are placed next to the target in order to detect the collision products that are scattered at large angles.

When one or several nucleons are removed from a nucleus the resulting fragment may be unstable due to the resulting holes in its single-particle orbitals. The nucleus could then, as a result, evaporate one or many nucleons after the collision in order to return to a state with lower excitation energy. The time between collision and evaporation in such cases is typically very small. Hence, the evaporation does likely take place while the ion is still travelling through the atom layers of the target. After exiting the XB-detector the main fragments and the nucleons that are ejected in the beam direction at the collision, as well as those evaporated by excited nuclei after the collision, pass through ALADiN.

ALADiN's task is to separate the reaction products in terms of magnetic rigidity. The typical trajectories of neutrons, ions and protons are also illustrated in Figure

1. The process is described in more detail in Section 2.3. The uncharged neutrons are not affected by the magnetic field of ALADiN and hence travel straight through the setup. The neutrons are detected by the Large Area Neutron Detector (LAND), which measures position and time of flight of the neutrons in order to determine their 4-momenta.

Naturally, the trajectories of protons, which have a high charge relative to their mass, are bent the furthest by the magnet. The positions of the protons are detected by the Proton Drift Chambers (PDC) and again by the Dicke ToF-wall (DTF), which determines their position, time of flight and energy loss.

In the same manner the unreacted and reacted ions travel through the magnet in trajectories that are determined by their respective magnetic rigidity. After exiting the magnet, the ions pass through two GFI-detectors, which measure position in the bending direction. The ions then reach the final detector, TFW, which measures positions both vertically and horizontally, as well as time and energy loss.

As stated in Section 1.1, our task is to find the detection limits for the ions as they travel through the setup. Therefore only the fragment arm of the setup is of interest for this project.

## 2.2 Three Detectors of Special Interest

The three detectors that are of particular interest for this project are the SST, GFI and TFW detectors. As has been described in the section above (Section 2.1) the experimental setup consists of eight SST-detectors placed near the target, of which the two after the target are of interest to us. Downstream of the ALADiN-magnet there are two GFI-detectors and one TFW-detector that are of importance for our project. In this section a more detailed description of these detectors of interest is given.

### 2.2.1 Silicon Strip Detectors, SST

The SST-detectors in front of the target are used to measure energy loss and position of the incoming ions and those after the target do that for reaction products and unreacted beam ions [4]. The principle of the detection method is based on the ability of the ions to excite electrons in the semi-conducting material of the detector. As ions travel through the detector, they excite valence electrons in the material along their path. By applying a voltage across the detectors, these electrons, now in the conduction band, move to the anode of the detector. This results in current pulses, which are passed through amplifiers after which they reach an Analog to Digital Converter (ADC). This provides the deposited energy of the beam to a data acquisition system.

The energy deposited in the material is proportional to the square of the atomic number of the ion, as can be seen in Equation 3 in Section 2.3. Hence this value can

be used to determine what charge the ion passing the detector had.

SST-detectors consist of silicon strips that act as individual detectors. These silicon strips are placed in two layers, one with horizontal strips and one with vertically placed strips. That means that SST-detectors detect both the horizontal and vertical positions of an incoming particle by knowing what strip it passes through. The strip pitch and the resulting position resolution of the SST-detectors in the LAND/R<sup>3</sup>B-setup is approximately 0.1 mm.

### **2.2.2 Großer Fiberdetektors, GFI**

GFI-detectors detect positions of incoming particles in the horizontal plane, only. The detectors consist of many scintillator-fibers positioned vertically next to each other. In the material of the scintillators there are certain allowed electron energy states. As an ion travels through the scintillator material it excites electrons along its path to states of higher energy. The excited electrons thereafter fall to states of lower energy, i.e. higher stability, under emission of photons. This results in light pulses in the scintillators. There is cladding around the fibres to protect them from external light. By registering the light pulses it is known through which scintillator each particle passes, hence the particles position can be extracted.

In the GFI-detectors in the LAND/R<sup>3</sup>B-setup, the side length of each scintillator is 1 mm. Therefore the resolution of the GFI-detectors is in the region of 1 mm. The width of the plane of detectors is 50 cm.

### **2.2.3 Time of Flight Wall, TFW**

The TFW detects position, energy and time of detection in the LAND/R<sup>3</sup>B-setup. It consists of two planes of scintillator paddles, in which the scintillators are placed vertically and horizontally. Therefore the TFW-detector provides information on the position in both directions, by placing photo-multiplier tubes on both ends of a scintillator bar.

By measuring the time of detection at the TFW-detector, and comparing this to the start values provided by the POS-detector at the beginning of the setup, the time of flight is obtained. Furthermore, the TFW detects energy deposited by the ions. This is done through measuring the amount of the emitted light in the scintillators. The Bethe-Bloch formula, that relates energy loss and atomic number, which is also used for the SST-detector signals can be used here as well to extract the charge of the ion. The active area of the TFW has a width of 180 cm and a height of 140 cm. Its position resolution is in the order of 5 cm.

## **2.3 Reconstruction of the Ions**

Quantities like the nuclear mass and charge of the ions can be reconstructed from the data provided by the three types of detectors discussed in the previous section.

From the set of detectors used, the positions of the ions is measured five times in the horizontal direction, which determines how much the trajectories of the ions are bent by the magnet. There are also three position measurements in the vertical direction, three points of known energy deposit, as well as the known time of flight of the ions from the start to the end of the LAND/R<sup>3</sup>B-setup. This section describes how the most interesting quantities for analysis, mass and momentum, are extracted.

For a particle moving in a magnetic field the magnitude of the force on the charge is proportional to its electric charge, as can be seen in the Lorentz force equation:

$$\vec{F} = q(\vec{E} + \vec{v} \times \vec{B}), \quad (1)$$

where  $\vec{F}$  is the force on a particle with charge  $q$  traveling with velocity  $\vec{v}$  under the influence of a magnetic field  $\vec{B}$  and/or electric field  $\vec{E}$ . In the case of the S393-experiment there was no electric field, hence  $\vec{E} = 0$ .

From Equation 1 it is clear that ions of larger electric charge experience a larger force from the magnetic field. The magnetic field of ALADiN is in the vertical direction in the LAND/R<sup>3</sup>B-setup and hence the force is in the horizontal direction, resulting in the bent trajectories of the reaction products in Figure 1.

In order to find an equation relating the magnetic rigidity to the momentum and charge the Lorentz equation can be used in the formula for circular motion, as can be seen in Appendix B. The derivation must be done relativistically since the velocities of the ions are larger than 10 percent of the speed of light. The following relation is derived

$$B\rho = \frac{\gamma\beta cm}{q} \propto \frac{A}{Z}, \quad (2)$$

where  $B\rho$  is the magnetic rigidity of the incoming ion,  $\gamma$  is the Lorentz factor,  $m$  is the mass of the ion and  $q$  is the charge of the ion. The velocity of the ion is  $v = \beta c$ , where  $c$  is the speed of light. The mass of the ion is proportional to the atomic mass number,  $A$ , of the ion. If the ions are completely ionized, as they are in the LAND/R<sup>3</sup>B-experiments, the charge of the ions is proportional to the atomic number  $Z$ .

However, for this equation to be useful in determining the mass and momentum of the ions in the S393-experiment, it is also necessary to know the charge (i.e. atomic number,  $Z$ ) of the incoming ions. In order to determine this, the interactions of the ions with the detector material in the SST-detectors and the TFW need to be considered. In these interactions the atomic number has an impact on the amount of energy deposited. The full formula relating the energy deposited,  $\Delta E$ , to the atomic number,  $Z$ , is called the Bethe-Bloch equation

$$\Delta E \equiv -\left\langle \frac{dE}{dx} \right\rangle = K Z^2 \frac{z}{a} \frac{1}{\beta^2} \left[ \frac{1}{2} \ln \frac{2m_e c^2 \beta^2 \gamma^2 W_{max}}{I^2} - \beta^2 - \frac{\delta(\beta\gamma)}{2} \right], \quad (3)$$

here  $Z$  is the charge number of the impinging ion, with a velocity,  $v = \beta c$ , and  $c$  as the speed of light.  $z$  and  $a$  are the atomic number and atomic mass number of the detector material.  $W_{max}$  is the maximum energy transfer at collision,  $I$  is the mean excitation energy,  $K$  is a constant and  $\gamma = \frac{1}{\sqrt{1-\beta^2}}$  is the Lorentz factor. The equation has been taken from the Particle Data Group [6].

The full derivation of this equation is too complicated to be included in this report. Instead the reader is referred to the Particle Data Group [6], or the book "Techniques for Nuclear and Particle Physics Experiments" by W. R. Leo [7], where the equation is described further.

From Equations 2 and 3, all the information necessary to identify the ions can be extracted. By performing a fit to the five points of horizontal position measurements the bending radius,  $\rho$ , of the ions can be deduced. By also knowing the size of the magnetic field,  $B$ , as well as the energy loss,  $\Delta E$ , the momentum and mass of the ions can be reconstructed. This is done by the program LAND/R<sup>3</sup>B-TRACKER, which is described further in Chapter 3.

## 2.4 Consequences of the Collisions

The S393-experiment alternated between three targets; carbon, plastic and lead. Since the space between atoms in the target is large relative to the size of the nuclei, and since the targets are thin, it is quite common for ions to travel through the target without interacting with its nuclei. However, in some cases collisions occur. These collisions give rise to different reactions.

A reaction mechanism of interest is the knock-out reaction. The key point for knock-out reactions is that for high energies the de Broglie wavelength,  $\lambda_{dB}$ , for a nucleon has about the same length scale as the size of a nucleon. Thus, there is a fair chance for the target nucleon to interact solely with one or two nucleons of the projectile. Such interactions happening at high energies may remove one or two protons or neutrons. In the case of projectile fragmentation several protons and neutrons in many combinations can get knocked out. These interactions are more complicated because more collisions are involved. Also, projectile fragmentation reactions typically result in the evaporation of nucleons [4][1].

Evaporation occurs when nucleons fill the vacancy in an orbital created by knocked-out nucleons. Thermalization of the resulting excitation energy distributes the latter to all available degrees of freedom. Statistically there is a possibility of one nucleon gaining sufficient energy to leave the system. This is called evaporation and result in a significantly lower recoil of the nuclei compared to a knock-out reaction [4][1].

Due to the preservation of energy and momentum the removal of a nucleon causes the ion to recoil in the opposite direction. The magnitude and direction of this recoil depend on the momentum of the removed nucleon [8]. Since we simulate the ion after the reaction we have to introduce recoil artificially, this is henceforth called

kick. Since the kick may be oriented in any direction it may add a transverse momentum to the ion, which is maximal if the kick is directed perpendicularly to the beam direction. As stated in the first chapter of this report, our task is to find the limit at which these kicks can make isotopes miss the detectors, or prevent correct reconstruction in any other way.

The magnitude of the kick is equal to the momentum of the particle removed. In a nucleus the nucleons have different momenta depending on their kinetic energy. In 2011 a PhD-thesis investigating the momentum of the protons in a  $^{12}\text{C}$ -ion was published by V. Panin [8]. Panin's results are used in this project to estimate the magnitude of kicks that are relevant for the S393-experiment. The process of calculating those kicks is described in the next chapter.

## 2.5 Half-lives of the Ions

In order to understand the possible outcomes of the S393-experiment, it is important to identify the ions that were used according to nuclear mass and charge. One central point is to take into account the properties of the daughter nuclei of these ions, especially their respective levels of stability. In the collision with a target nucleus, these nuclei may have lost one or several protons and/or neutrons. Furthermore, excitations of the daughter ions, as a result of the collisions, may have caused them to evaporate one or more nucleons. That means that the atomic mass number may have dropped by several units. The following table, Table 1, contains a list of half-lives of the isotopes in the region of interest to this project.

Table 1: Half-lives of the isotopes that were simulated. Data from National Nuclear Data Center [9].

Isotope	Half-life	Isotope	Half-life	Isotope	Half-life
$^{17}\text{C}$	193 ms	$^{17}\text{B}$	5.08 ms	–	–
$^{16}\text{C}$	747 ms	$^{16}\text{B}$	0.19 ns	$^{16}\text{Be}$	200 ns
$^{15}\text{C}$	2.449 s	$^{15}\text{B}$	9.87 ms	$^{15}\text{Be}$	200 ns
$^{14}\text{C}$	5 730 a	$^{14}\text{B}$	12.5 ms	$^{14}\text{Be}$	4.84 ms
$^{13}\text{C}$	stable	$^{13}\text{B}$	17.33 ms	$^{13}\text{Be}$	$2.7 \cdot 10^{-21}$ s
$^{12}\text{C}$	stable	$^{12}\text{B}$	20.20 ms	$^{12}\text{Be}$	21.49 ms
$^{11}\text{C}$	20.334 min	$^{11}\text{B}$	stable	$^{11}\text{Be}$	13.81 ms
$^{10}\text{C}$	19.290 s	$^{10}\text{B}$	stable	$^{10}\text{Be}$	$1.39 \cdot 10^6$ a
$^9\text{C}$	126.5 ms	$^9\text{B}$	$8 \cdot 10^{-19}$ s	$^9\text{Be}$	stable
–	–	$^8\text{B}$	770 ms	$^8\text{Be}$	$6.7 \cdot 10^{-17}$ s
–	–	–	–	$^7\text{Be}$	53.22 days

The flight times of the ions in the S393-experiment, measured from the target to the TFW, were in the order of tens of nanoseconds. By studying Table 1, it is clear the isotopes  $^8\text{Be}$ ,  $^{13}\text{Be}$ ,  $^9\text{B}$  and  $^{16}\text{B}$  are either unbound or have half-lives that are several magnitudes smaller than the typical flight times. Even taking relativistic effects into account the possibility of these isotopes reaching the detectors can be neglected. Hence  $^8\text{Be}$ ,  $^{13}\text{Be}$ ,  $^9\text{B}$  and  $^{16}\text{B}$  will not be simulated.

# 3 Simulations

In order to find the detection limit of the LAND/R<sup>3</sup>B-setup of the S393-experiment, simulations are used. Simulations are an important tool for analyzing and interpreting results from experiments. One important point of using simulations is that the input is known. The incoming fragments and their kinematic properties are selected as needed. Another advantage is that it is possible to know even where the particles that miss the detectors end up, whereas experimentally all that can be known is the information delivered by the detectors. Hence, the simulations give full control of all simulated ions. Furthermore, detectors in the simulations can be set to have perfect resolution before introducing the actual values from the detectors used in the LAND/R<sup>3</sup>B-setup. In that way the consequences of limited size and resolution of the detectors can be isolated, thereby clarifying the results. In the simulations and analysis three software tools, GGLAND, ROOT and LAND/R<sup>3</sup>B-TRACKER have been central to this project. These tools are described in Section 3.1.

The effects of varying transverse momentum on the efficiency are analyzed by simulating the experiment with different amounts of transverse momentum of the incoming fragments and comparing the number of entries in the individual detectors. Section 3.2 describes the process of finding a value for a realistic transverse momentum for the reactions. The last sections, Section 3.3, 3.4 and 3.5, describe the simulations used in the project as well as the analysis process. Because different isotopes will be affected differently by the transverse momentum the simulations were performed for several isotopes of interest to the S393-experiment.

## 3.1 Software Tools

The simulation and reconstruction tools that were used in this project are GGLAND (a command-line wrapper that uses GEANT4) and LAND/R<sup>3</sup>B-TRACKER. The simulations were conducted in the GGLAND/GEANT4 framework after which the simulation data was tracked using the program LAND/R<sup>3</sup>B-TRACKER. LAND/R<sup>3</sup>B-TRACKER reconstructs the path through the setup of the ions according to detected positions and therefrom determines quantities of interest to the experiment. The data were later analyzed in the program ROOT in which fits were made to the data in order to determine the amount of correctly tracked events.

### 3.1.1 GEANT4

GEANT4 is a toolkit for simulating high energy particle and nuclear experiments. The toolkit uses a wide range of physical models and factors to be taken into consideration in simulating the events. These are defined in a list, referred to as a

”physics list”. The physics list used for this project was QGSP\_BERT. When performing a simulation the software randomly selects processes that can take place based on their defined probability in the listed models. The statistical method used by GEANT4 is a Monte Carlo method, that is a stochastic method using random numbers to generate the distribution [10]. In this project version 10.01 of GEANT4 was used.

### 3.1.2 GGLAND

GGLAND is a wrapper made to simplify the use of the GEANT3 and GEANT4 simulations tools [11], developed by Håkan Johansson at Chalmers University of Technology. GGLAND operates using a command-line interface where the experiment can be modeled. There it is possible to declare position, rotation and type of various predefined detectors, environments and particle-guns. A particle-gun spawns particles with a defined velocity and direction. Furthermore, *.root*-files, containing data, can be produced by these simulations. More information about GGLAND is available in Håkan Johansson’s documentation on GGLAND [12].

### 3.1.3 LAND/R<sup>3</sup>B-TRACKER

In order to reconstruct the paths of the different ions in the simulations, a software called LAND/R<sup>3</sup>B-TRACKER was used. LAND/R<sup>3</sup>B-TRACKER is a tool, developed by Ralf Plag at GSI, that tries to reconstruct both experimental data and simulated data by comparing the data gathered from the detectors to the equations of motions of a particle moving through a magnetic field. The tracker calculates numerous paths and chooses the one that minimizes the  $\chi^2$ -test. A  $\chi^2$ -test is a standard method that associates different weight function to different data points and then tries to minimize the error from the measured data compared to some calculated data.

To use the LAND/R<sup>3</sup>B-TRACKER it must be provided with data from a *.root*-file. The tracker must also be provided with the values for the mass, charge and velocity of the incoming ion. Furthermore, the tracker must be given the charge of the ion that hits the TFW. The velocity was calculated according to Equation 11 of Appendix B. Finally an energy interval for ions at TFW in the *.root* file has to be specified. The tracker only tracks ions with energy within this interval because the other energies do not originate from the simulated ions hitting the TFW, and disturb the tracking.

The tracking mode used in this project was forward tracking. This means two detectors before ALADiN, in our case two SST-detectors were used to fix the track position.

### 3.1.4 ROOT

For data analysis ROOT was used. ROOT is a CERN-developed software framework, mainly written in C++. It is able to handle large amounts of data. That

makes it suitable for the simulations of this project. Furthermore, both GGLAND and LAND/R<sup>3</sup>B-TRACKER produce data in ROOT's own file format, ROOT-files, *.root*.

ROOT has been used in generating the spectra analyzed in this project. For this purpose, ROOT version 6 was used. In analyzing the results, a script was written in C++ to fit a Gaussian function to a mass histogram and calculating the integral of said function over an interval. This program was written for and used in ROOT version 5. It was used for finding the detection efficiency of the setup.

## 3.2 Elimination of Paddle Spacing in TFW

In defining the detectors in GGLAND, the TFW was changed. The TFW consists of horizontal and vertical paddles that detect ions. For an ion to be detected, it has to hit at least one of the paddles. These paddles have a gap between them that intersect at 221 positions, giving rise to squares of area  $0.04 \text{ cm}^2$ , each, where the ions can not be detected. In the simulations of this project, the size of the paddles were changed so that the gap between them was eliminated. This was necessary due to read-out problems otherwise created in the simulation. This resulted in a TFW that was equally large as the real TFW but without any gaps in its detection area. The removed space had a total area of  $221 \cdot 0.04 = 8.84 \text{ cm}^2$ , and the total area of the TFW was  $26\,153 \text{ cm}^2$ . This means around 0.034 % of the detected hits in the simulations would not have been detected had it been a real experiment.

## 3.3 Deriving a Realistic Kick

As has been mentioned in Chapter 2, the removal of a proton or neutron at collision results in the fragments experiencing kicks. The magnitude and direction of the kick depends on the momentum of the lost nucleons as well as on the impact parameter of the collision. In order to derive the typical magnitude of these kicks to be used in the simulations, information from a PhD thesis published by V. Panin [8] was used.

In chapter four of Panin's PhD thesis "Fully Exclusive Measurements of Quasi-Free Single-Nucleon Knockout Reactions in Inverse Kinematics" measurements of the internal momenta of p- and s-orbital protons are presented. The main information of concern when determining the kick is the  $\ell$  quantum number, the orbital angular momentum, a nucleon has. Panin shows that the internal momentum in any arbitrary direction for protons in a p-orbital of a  $^{12}\text{C}$  atom is a distribution with a maximum of about  $350 \text{ MeV}/c$  and a distribution with a maximum of  $400 \text{ MeV}/c$  in s-orbitals. It is approximated for the purposes of this report that these values are the same for knocked-out neutrons and regardless of the parent ion, even though there is a slight difference. Different nuclei will have varying amounts of p- or s-state nucleons, meaning the probability to knock out a p- or s-state nucleon, or indeed a d-state nucleon, varies with how the different nucleons fill up the nuclear orbitals.

The process of nucleon removal has an effect on the projectile according to momentum conservation. The nucleons that leave the nucleus do so in random directions,

as there is no preferred direction. If the projectile undergoes a knock-out reaction, its momentum is changed equally much in the opposite direction of the internal momentum of the knocked out nucleon. The kick defined in GGLAND has to be in the zero-momentum (ZM) frame of the system and Panin's results are in the lab frame.

However, in the case that the velocity of the nucleon is perpendicular to the velocity of the beam, we arrive at the formula for velocity addition, perpendicular to the velocity of the frames

$$v = \sqrt{1 - \beta^2} v' = \gamma^{-1} v' \Leftrightarrow p = \gamma m v = m v', \quad (4)$$

where the ZM frame is moving with velocity  $\beta c$  and  $v'$  is the perpendicular velocity in the lab frame. This means that no relativistic effects arise. Since this case presents the highest change in transversal momentum for the fragment, it suffices to assume that all other possibilities involve lower transversal momenta. Meaning the internal momenta of interest that could affect the beam are below the maximum internal momentum in any direction for the nucleons. It is shown in Figure 7, in Chapter 5, that introducing kicks lower than 400 MeV/c does not affect the efficiency considerably if the beam spot is fairly centered, which is the case for most ions. Since the introduction of a kick increases the size of the beam spot, the closer the beam spot is to the edge of the detectors, the more efficiency is typically lost when adding a kick. There are some cases where investigating kicks below 400 MeV/c would be interesting, however, this project covers only the maximum possible amount of kick per nucleon removed, that is 400 MeV/c.

### 3.4 Simulation Method

The particle-gun and detectors of the simulated experiment were placed in a simulated volume by specifying positions and rotations. Appendix C lists the exact positions of the detectors. The gun was shaped like a square, emitting ions in the  $z$ -direction, to resemble the beam after the target of the experiment. The simulated ions were produced by the gun with velocities  $\beta c$  for  $\beta$  values between 0.72 and 0.76. To simulate the recoil, the ions were kicked with 400 MeV/c per nucleon in random directions in the ions rest frame. The simulations presented in this report are from 300 000 or 1 000 000 simulated ions each.

Having a perfect resolution is possible when running simulations. In real experiments however, it is not. Adding the uncertainties of the detectors to the data was performed in GGLAND by adding a random value from a normal distribution to the data from each detector based on their respective resolution.

The simulations resulted in *.root*-files that contained data from the simulations. To reconstruct quantities like the mass and 4-momentum of the ions, the software tool LAND/R<sup>3</sup>B-TRACKER was used. The *.root*-files from the simulations were tracked and the resulting *.root*-files were then used for determining the efficiencies for each simulation.

### 3.5 Data Analysis

In ROOT, histograms of the generated data were studied, such as where the ions hit the detectors, their energies, time of flight and mass. By looking at hit positions for the ions at individual detectors, it was possible to discern which detectors some of the ions missed, limiting the detection efficiency of the experimental setup.

In order to determine the efficiency for each reaction channel, a normal distribution of the masses of the ions at the end of the setup was assumed to be physically correct. To sort the successful simulations from those that misreconstructed, a Gaussian function was fitted to the histogram of the fragment masses. The integral of this Gaussian in the interval mean minus four standard deviations to the mean plus four standard deviations is assumed to cover all properly tracked events of a given mass, see Equation 5.

$$N = \int_{\mu-4\sigma}^{\mu+4\sigma} G dx, \quad (5)$$

where  $N$  is the number of correct reconstructions,  $\mu$  the mean,  $\sigma$  the standard deviation and  $x$  is the mass.  $G$  is the Gaussian function that was fitted to the histogram of the form

$$G = H e^{-\left(\frac{x-\mu}{\sqrt{2}\sigma}\right)^2}, \quad (6)$$

where  $H$  is the height. In this way, the efficiencies,  $\epsilon$  were determined by the number of properly tracked events per simulation. If  $M$  is the total number of simulated events, the efficiency is

$$\epsilon = \frac{N}{M}. \quad (7)$$

After the efficiencies were determined, data were written into a *.m*-file in MATLAB and plotted into figures presented in the next chapter. Tables of efficiencies were also created and are presented in Appendix A.

# 4 Results

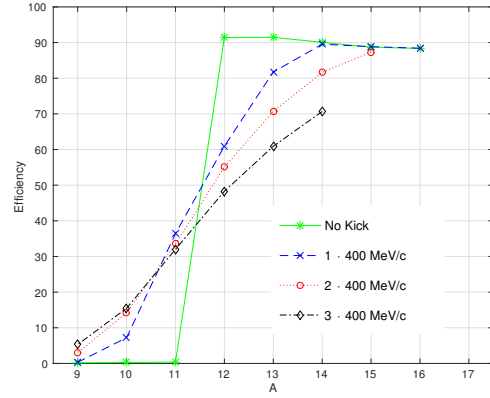
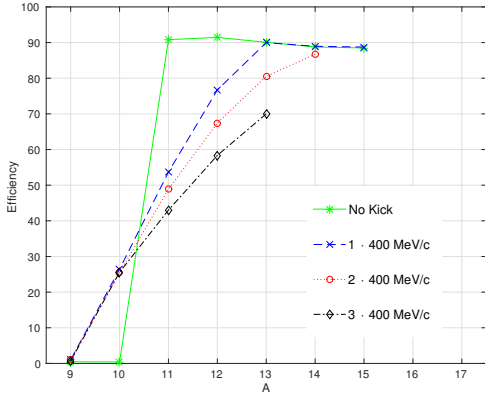
The simulations of the project resulted in nine series of efficiency data. Three carbon isotopes,  $^{16}\text{C}$ ,  $^{17}\text{C}$  and  $^{18}\text{C}$ , were chosen as incoming ions with constant  $B\rho$ . This means the daughter isotopes had a  $\beta$  of 0.76, 0.74 and 0.72, respectively. See Equation 11 for a relativistic formula for calculating these values. Daughter fragments of carbon, boron and beryllium were simulated from each parent ion. For each fragment, simulations without any added momentum and with added momenta from one, two or three knocked out nucleons were made. Each nucleon adds a momentum of 400 MeV/c to the ion in a random direction. Simulations were conducted for each isotope from the parent ion down to  $^9\text{C}$ ,  $^8\text{B}$  and  $^7\text{Be}$ , with the exception of the unbound or highly unstable nuclei  $^{16}\text{B}$ ,  $^9\text{B}$ ,  $^{13}\text{Be}$  and  $^8\text{Be}$ . Kick from two and three nucleons were not simulated for the fragments which had exactly one or two nucleons less than their parent ion, respectively. In this chapter these data are presented in nine plots, one for each of the three series of each of the three parent ions. See Tables 2, 3 and 4 for tables of all efficiency data.

## 4.1 Carbon Fragments

As can be seen in Figures 2a, 2b and 2c, the efficiency of carbon fragments with a kick of zero is approximately constant around 90 % for all masses higher than a specific mass. This pattern holds true for all parent isotopes. The efficiency drops at higher masses with increasing parent mass and decreasing velocity. This drop off is located below  $A = 11$  for parent isotope  $^{16}\text{C}$ , at  $A = 12$  for  $^{17}\text{C}$ , and at  $A = 13$  for  $^{18}\text{C}$ .

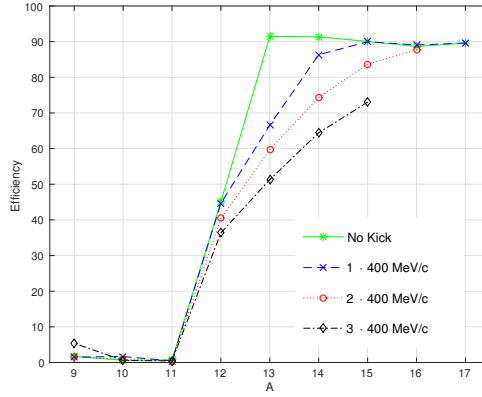
With kick, a more gradual decrease of efficiency is observed, as can be observed in Figure 2a. The efficiency decrease starts at a higher mass. Similar to simulated data without kick we can see that the drop-offs start at higher masses for fragments with higher parent mass. For one removed nucleon, the drop starts below  $A=13$  for the parent isotope  $^{16}\text{C}$ , below  $A=14$  for  $^{17}\text{C}$  and below  $A=15$  for  $^{18}\text{C}$ . Increasing the number of removed nucleons increases the starting mass of the drop-off, as can be seen in Figure 2c where the simulations with one removed nucleon start to drop below  $A=14$ , while those with two start to drop below  $A=16$ .

In Figure 2a it can be observed that efficiency of the ions without added momentum drops off sharply between  $^{11}\text{C}$  and  $^{10}\text{C}$ , while the ions with added momenta drop off more gradually. Note that the beam is much more focused for the ions without added momentum than those with, as can be seen in Figures 7a, 7b, 8a and 8b.



(a) Efficiencies of fragments of carbon produced in reactions from a beam of  $^{16}\text{C}$ .

(b) Efficiencies of fragments of carbon produced in reactions from a beam of  $^{17}\text{C}$ .



(c) Efficiencies of fragments of carbon produced in reactions from a beam of  $^{18}\text{C}$ .

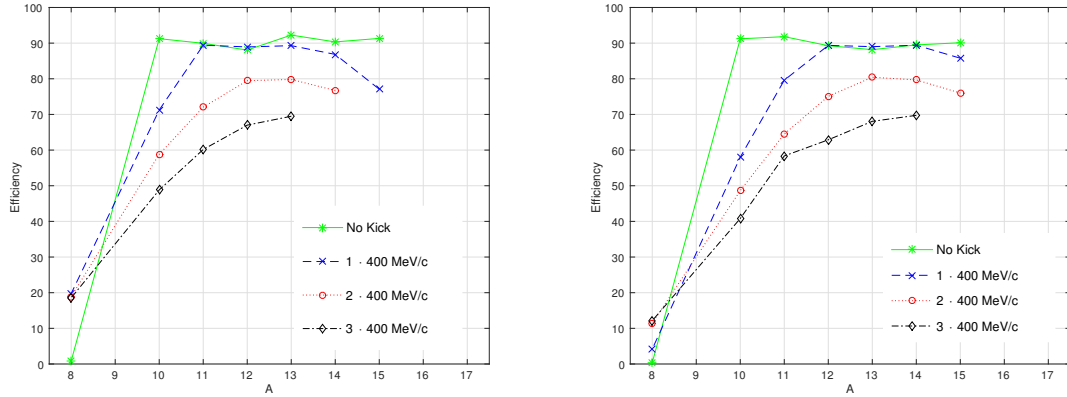
Figure 2: Efficiencies of fragments of carbon produced in reactions from different beams of carbon isotopes. The ions without kick exhibit sharp drop-offs in their efficiency for sufficiently low masses, while the ions with added momenta from knocked out nucleons show more gradual decrease for decreasing mass.

## 4.2 Boron Fragments

In Figures 3a, 3b and 3c the efficiencies of boron fragments with parent isotopes  $^{16}\text{C}$ ,  $^{17}\text{C}$  and  $^{18}\text{C}$ , respectively, are presented. As can be seen, the efficiencies of the boron fragments follow a similar pattern as the carbon fragments. Zero-kick fragments have a clear drop off for each of the parent ions  $^{16}\text{C}$ ,  $^{17}\text{C}$  and  $^{18}\text{C}$ .

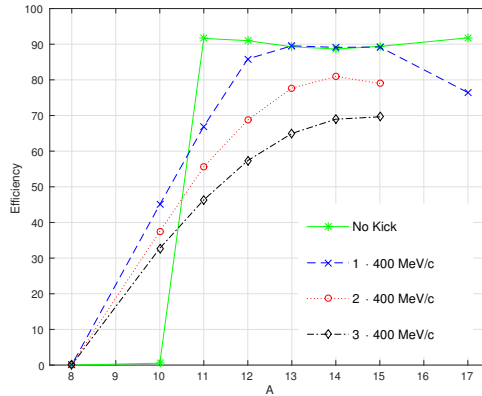
The ions that have had nucleons knocked out show a pattern in that they decrease gradually in efficiency as the mass decreases. In Figure 3a it is shown that the efficiency for simulations with one removed nucleon starts to drop below  $A=11$ , and for the other parent ions it starts at  $A=12$  and  $A=13$  for  $^{17}\text{C}$  and  $^{18}\text{C}$  respectively. The simulations with two and three knocked out nucleons follow similar patterns. This is very much like the carbon fragments. They also seem to drop in efficiency

for higher masses.  $^{14}\text{B}$  has higher efficiency than  $^{15}\text{B}$  for ions from  $^{16}\text{C}$  with one removed nucleon. This is because the higher magnetic rigidity causes the beam to reach the edge of the GFI detector on the other side than for low masses as is shown in Figures 9a and 9b. That is the reason behind the concave shapes in the plots.



(a) Efficiencies of fragments of boron produced in reactions from a beam of  $^{16}\text{C}$ .

(b) Efficiencies of fragments of boron produced in reactions from a beam of  $^{17}\text{C}$ .



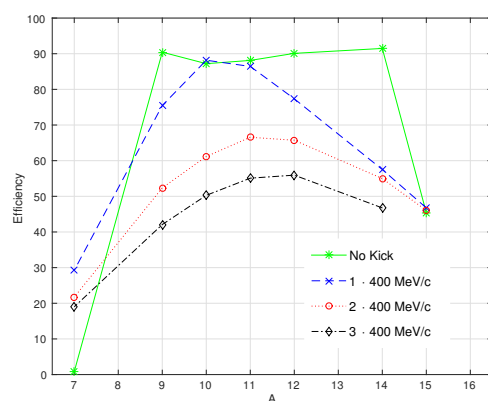
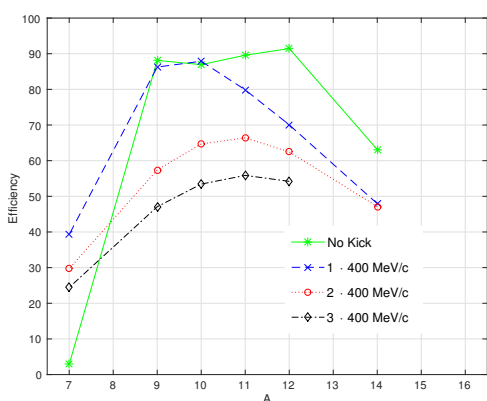
(c) Efficiencies of fragments of boron produced in reactions from a beam of  $^{18}\text{C}$ .

Figure 3: Efficiencies of fragments of boron produced in reactions from different beams of carbon isotopes. The ions without kick exhibit significant drop-offs in their efficiency for sufficiently low masses, while the ions with added momenta from knocked out nucleons show more gradual decrease for decreasing mass. The ions with added momenta from one and two knocked out nucleons show a small drop for high masses as well.

### 4.3 Beryllium Fragments

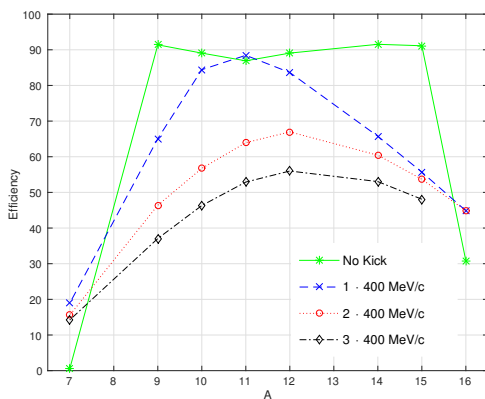
In Figures 4a, 4b and 4c efficiencies of beryllium fragments with parent isotope  $^{16}\text{C}$ ,  $^{17}\text{C}$  and  $^{18}\text{C}$  can be seen. For beryllium, patterns similar to those of carbon and boron fragments appear. One of the most striking differences is that efficiency drops for sufficiently low and high masses, even for the simulations without kick.

For the simulations from parent ion  $^{16}\text{C}$ , it can be observed, see Figure 4a, that the drop-offs for the ions without kick start below  $A=9$  and above  $A=12$ , and for those with one removed at below  $A=9$  and above  $A=10$ . The simulations with two or three nucleons removed seem to have maxima for efficiency at  $A=11$  and decrease on either side. This gives these plots a concave shape that is caused by the beam reaching both the left and right edges of the GFI2-detector, similar to Figures 9a and 9b. Very similar patterns are shown for the simulations with parent ions  $^{17}\text{C}$  and  $^{18}\text{C}$  as can be observed in Figures 4b and 4c.



(a) Efficiencies of fragments of beryllium produced in reactions from a beam of  $^{16}\text{C}$ .

(b) Efficiencies of fragments of beryllium produced in reactions from a beam of  $^{17}\text{C}$ .



(c) Efficiencies of fragments of beryllium produced in reactions from a beam of  $^{18}\text{C}$ .

Figure 4: Efficiencies of fragments of beryllium produced in reactions from different beams of carbon isotopes. These ions all exhibit drops in efficiency for high and low masses, meaning the beam spot reach both edges of the limiting detector GFI2. This gives these plots concave shapes.

# 5 Discussion

In this section, several topics are discussed, including the maximum efficiency, the effects of removal of nucleons, which detectors are hit and missed, how the kicks affect the efficiencies and spot sizes of the beams and how they relate to the magnetic rigidities,  $B\rho$ . Some error sources, that may have affected the results of this project, are also discussed.

## 5.1 Limiting Detectors

One important question is which detector limits the reconstruction. In Figure 5a a histogram showing the registered  $x$ -positions on the GFI2-detector for tracked fragments of  $^{12}\text{C}$  without kick is plotted. A sharp drop off at the left side of the histogram is seen, indicating that the beam spot is partially cut by the edge of the GFI2-detector. Figure 5b shows a histogram of the registered  $x$ -positions on the TFW for the same simulation. On this histogram no sharp drop off is observed, indicating that the entire beam spot fits the TFW. This indicates that the limiting detector is the GFI2-detector, since the data from all the other detectors shows similar results to the TFW.

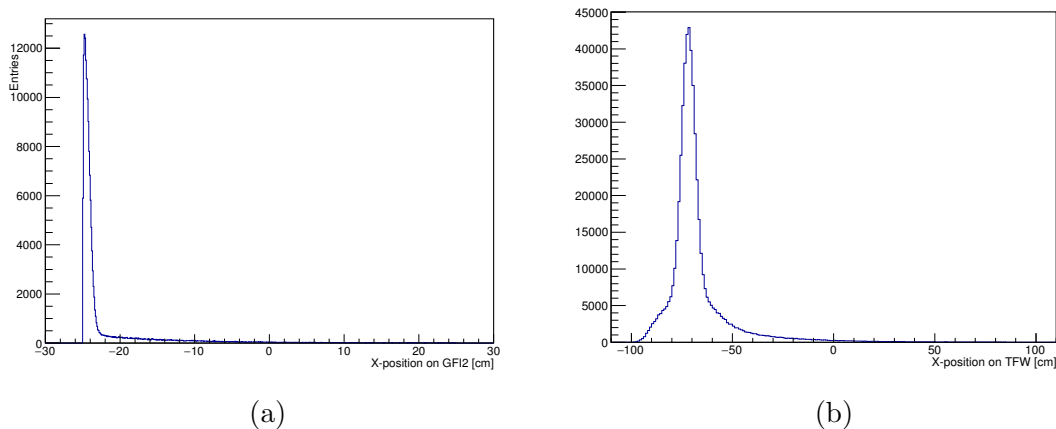


Figure 5: Histograms showing the registered  $x$ -positions on GFI2 (a) and TFW (b) for simulated  $^{12}\text{C}$  with parent ion  $^{17}\text{C}$ .

## 5.2 Maximum Efficiency

The maximum efficiency reached is approximately 90 %. This is seen for beams without kick but also for some cases of added transversal momentum from one removed nucleon. It can be noted for all fragments with high efficiency that the number of entries for each detector increases along the beam direction. For  $^{15}\text{C}$  with parent

isotope  $^{17}\text{C}$ , for example, the number of entries for GFI1 is 440 913 and for GFI2 the number of entries is 455 097. This implies that reactions happen in-flight through the air, and at detectors upstream, that produce products detected by detectors downstream.

The reactions mentioned above should all decrease the overall efficiency since the fragments reacting with the air or detector layer are deflected, and could therefore miss detectors. It is hard to conclude from our data how much each reaction contributes to the decrease in efficiency, but they should contribute with a significant part of the efficiency decrease of the maximum efficiency. Furthermore, the detectors themselves do not have perfect detection efficiency. For example the GFI detectors have cladding which further decreases the maximum efficiency.

### 5.3 Limitations of the Tracker

The tracker used in this project works by calculating different paths through the detector setup and chooses the one that minimizes  $\chi^2$ . It can happen that the path chosen differs between measured and tracked positions. This is reflected in the residuals. For large residuals, the calculated mass of the ions deviates from what is expected. This is illustrated in Figure 6, where  $\chi^2$  is plotted against mass of an ion. As can be observed, increased values of  $\chi^2$ , and therefore increased residuals, make for significantly deviating masses. Since the efficiency was determined assuming a normal distribution, the tracking results with high residuals were discarded, resulting in a lowered maximum efficiency.

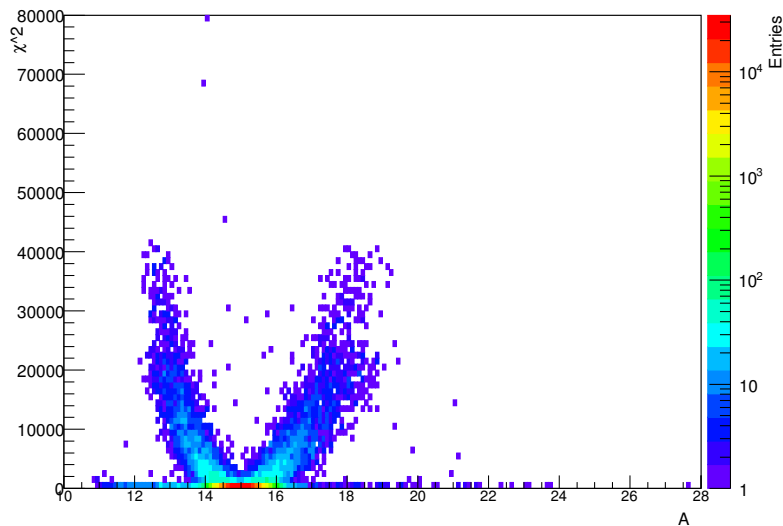


Figure 6:  $\chi^2$  plotted against mass of  $^{15}\text{C}$  ions produced from a beam of  $^{17}\text{C}$  without any kick. Higher values of  $\chi^2$  result in masses, which differ from the correct one.

## 5.4 General Effects of Transversal Momentum

Ions unaffected by transversal momentum transfer form a focused and narrow ion beam. The simulated beam disperses only slightly on its trajectory. A focused beam without added transversal momentum impinging on the TFW can be observed in Figure 7a. The vast amount of hits are concentrated in a narrow circular area marked by red color in the figure.

Introducing transversal kick greatly increases the dispersion of the beam, leading to a beam spot with larger radius at the detectors in the setup. In Figures 7b, 8a and 8b beams affected by added momentum from one, two and three removed nucleons can be observed. The beam radius increases with increasing number of nucleons introducing kick. This increase in beam dispersion leads, in most cases, to a decrease in efficiency as the ions affected by a large transversal kick can miss the detectors. The kick can also make ions hit detectors which had otherwise been missed. The effects of kick are especially significant for ions with added momenta from more than one removed nucleon.

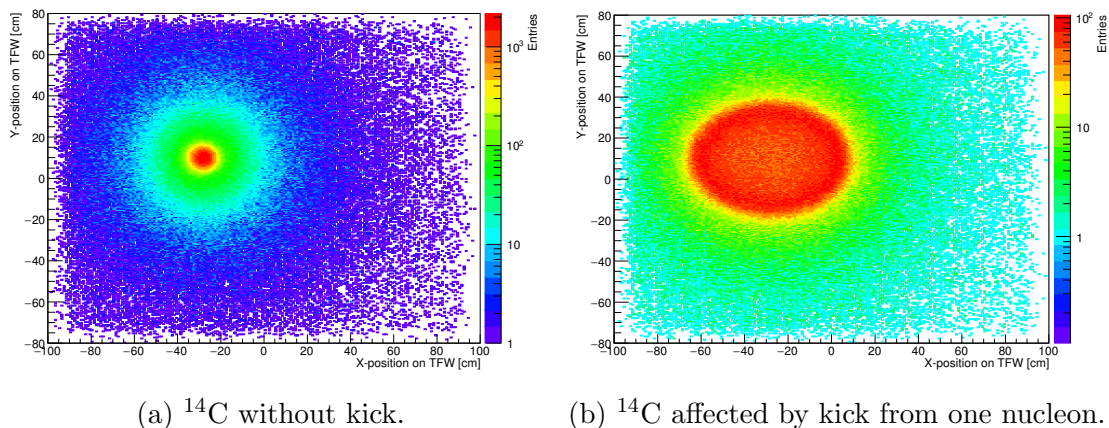
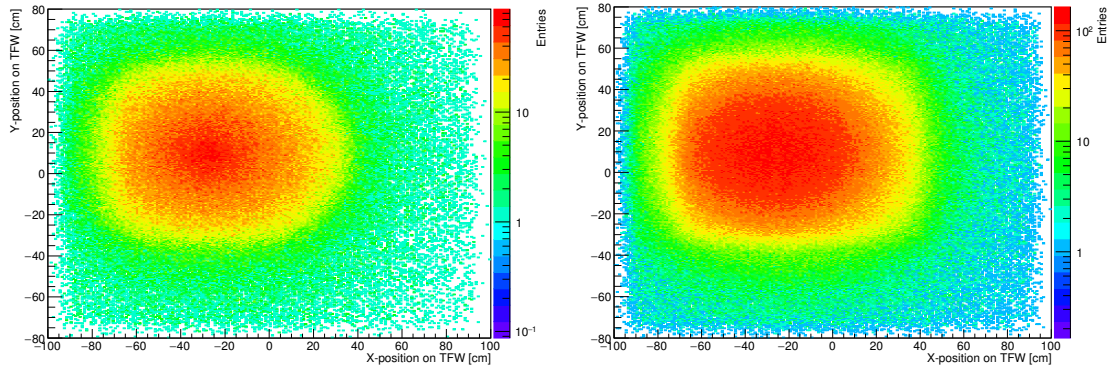


Figure 7: Histograms showing the positions of detected hits at the TFW for a simulated  $^{14}\text{C}$ -beam running through the LAND/R<sup>3</sup>B-setup.



(a)  $^{14}\text{C}$  affected by kick from two removed nucleons. (b)  $^{14}\text{C}$  affected by kick from three removed nucleons.

Figure 8: Histograms showing the positions of detected hits on the TFW for a simulated  $^{14}\text{C}$ -beam passing through the LAND/R<sup>3</sup>B-setup. The added transversal momentum is 400 MeV/c.

In Figure 2b it can be observed that the efficiency of the setup for fragments affected by kick from one nucleon is the same as those without kick. This implies that for these values the one-nucleon recoil does not disrupt the ion beam enough to cause it to miss detectors. Figure 7b shows a  $^{14}\text{C}$ -beam affected by added momentum from one removed nucleon impinging on TFW. Since the entire beam spot fits the detectors, the  $^{14}\text{C}$ -beam with a kick from one nucleon does not exhibit a decrease in efficiency compared to  $^{14}\text{C}$  without kick, whose beam spot on the TFW-detector is plotted in Figure 7a.

## 5.5 Missing the GFI2-detector

It can be observed that the efficiency decreases with sufficiently high or low masses, as seen in, for example, Figure 3a for boron fragments with a recoil of 400 MeV/c. As can be seen in Figures 9a and 9b, the lighter nuclei,  $^{10}\text{B}$ , are more deflected by the ALADiN magnetic field and start to miss the GFI2-detector in the positive  $x$ -direction according to Figure 1. The heavier  $^{15}\text{B}$  fragments are affected to a smaller degree by the ALADiN magnetic field, leading to the beam reaching the detector position at a more negative  $x$ -value<sup>2</sup> according to the frame of Figure 1. The kick increases the spread of the fragment beam leading to part of the beam missing the GFI2-detector in this case.

<sup>2</sup>Note that the  $x$ -axis in the coordinate system of the setup and the GFI-plots are opposite in sign.

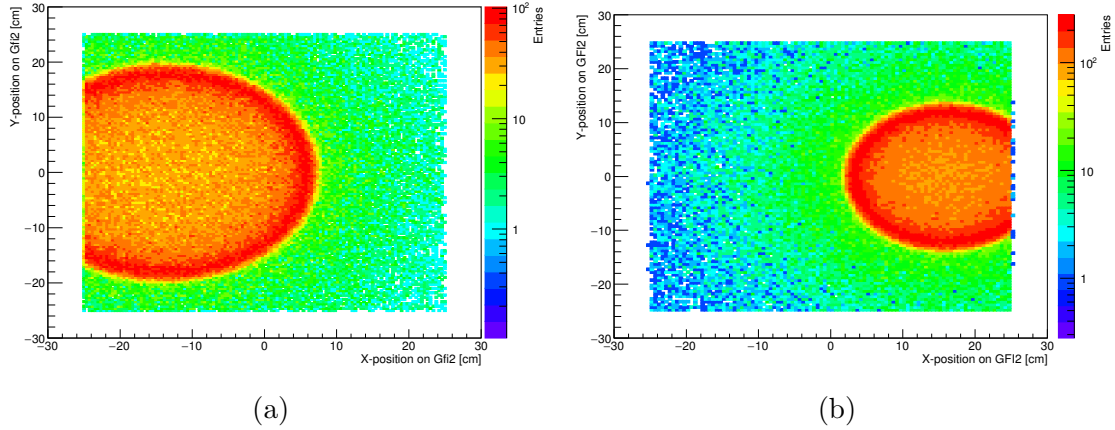


Figure 9: Hit positions on the GFI2-detector for  $^{10}\text{B}$  (a) and  $^{15}\text{B}$  (b). Part of the beam misses GFI2 on the left side for  $^{10}\text{B}$ , while for  $^{15}\text{B}$ , part of the beam misses it on the right side.

## 5.6 Increasing Efficiency with Kick

As can be noted from Figure 2a the fragment isotope  $^{10}\text{C}$  produced from the reaction of a  $^{16}\text{C}$  beam has higher efficiency when momentum is added compared to a situation without kick. This means ions with added momentum hit the detectors, which would not have been hit otherwise. As can be seen in Figures 10a and 10b it seems as though the beam misses the GFI2, but the added transversal momentum steers some of the ions back into the detector, as can be seen from the semi-circular shaped zone of hits. However, if the beam misses the detector by a too large margin, the kicks are not sufficient to allow for the ions to hit the detector, as can be seen in Figure 2a for  $^9\text{C}$ . This is illustrated in Figures 11a and 11b.

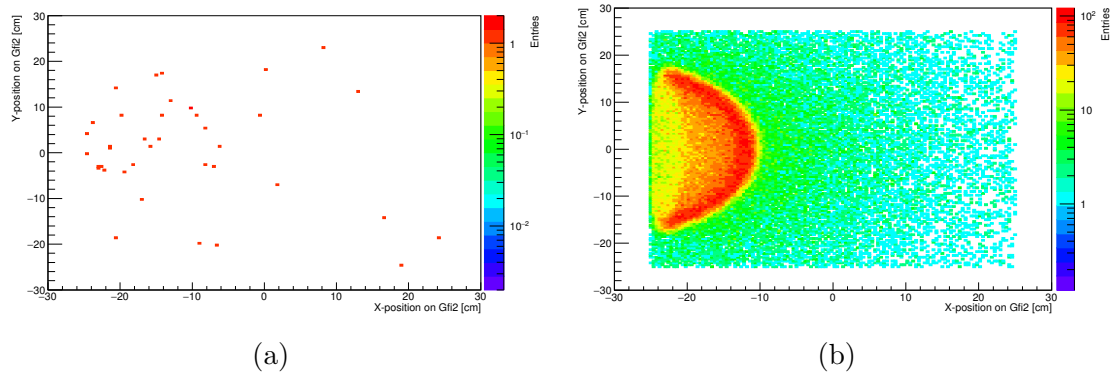


Figure 10: Histograms of hit positions at GFI2 for  $^{10}\text{C}$  fragments, produced from an incoming  $^{16}\text{C}$  beam, with kick from the removal of zero (a) and one (b) nucleon. Not many ions hit GFI2 in the unkicked case, because the beam misses the detector. Meanwhile the kick causes ions to hit the detector as the beam spot is much wider. This can be seen from the semicircular hit pattern that stems from part of the beam. See Figures 7a, 7b, 8a and 8b for beam size dependence as function of the added transversal momentum.

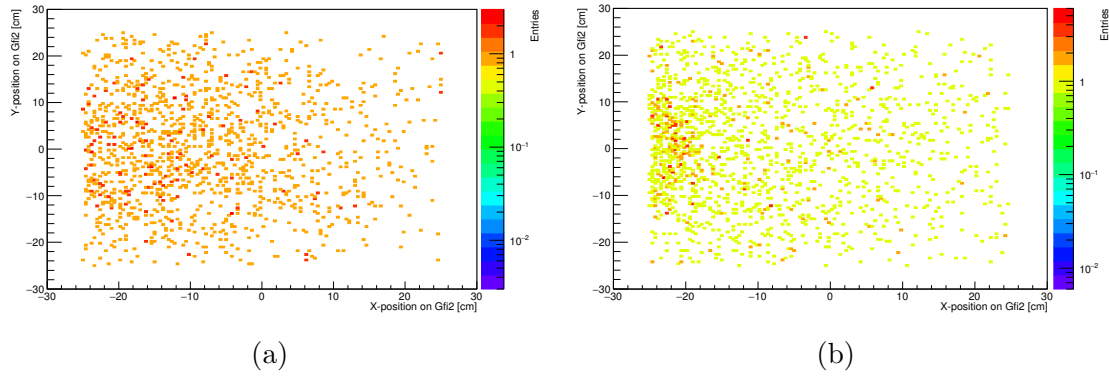
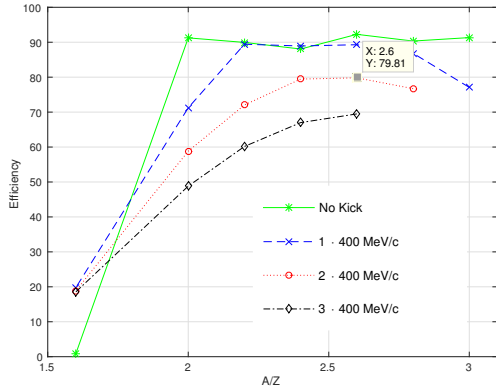


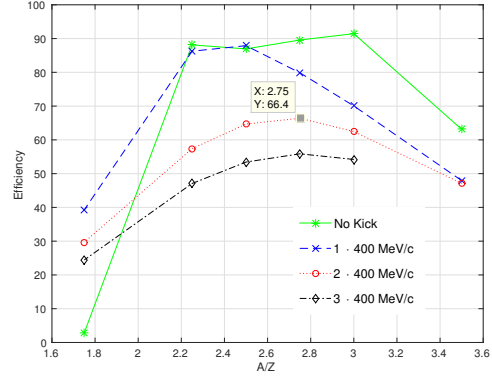
Figure 11: Histograms of hit positions at GFI2 for  ${}^9\text{C}$  fragments, produced from an incoming beam of  ${}^{16}\text{C}$ , with zero (a) and one (b) nucleon removed. In this case the kick is not sufficient to cause a clear hit pattern; because the center of the beam misses the detector by a too large margin.

## 5.7 Dependency of $A/Z$ on Beam Direction

The trajectory of the ions is largely dependent on how they are affected by the magnetic field in ALADiN. The ions change direction in ALADiN and move in a circular path because they move perpendicular to the magnetic field, see Equations 9 and 10. Because the magnetic field strength is constant, a good way to measure how ions are affected by the magnetic field is the magnetic rigidity,  $B\rho$ . See Equation 11. The experimental setup was optimized for a  $B\rho$  corresponding to that of  ${}^{17}\text{C}$  at a velocity of  $v = \beta c = 0.74c$ . Accordingly,  $\beta$  was calculated for  ${}^{16}\text{C}$  and  ${}^{18}\text{C}$  to be 0.76 and 0.72 respectively. From Equation 2 it is known that  $B\rho$  is roughly proportional to  $A/Z$ , the number of nucleons divided by the number of protons in an atom. Therefore, the optimal relation  $A/Z$  changes when varying  $\beta$ . By varying the relation  $A/Z$ , the flight path of the ions change. Different  $B\rho$  give different directions of the beams after ALADiN therefore the bending radius,  $\rho$  varies. This causes the beams to miss or hit the detectors which affects the efficiency. This means for a constant  $\beta$ , different ions should have peak efficiency for a certain  $A/Z$  even if their masses differ. This is illustrated in Figures 12a and 12b.



(a)



(b)

Figure 12: Efficiencies of boron (a) and beryllium (b) with same velocity,  $v = \beta c$ , plotted against  $A/Z$ . The marked points are the peak efficiencies for the ions with two removed nucleons. Note that these peaks occur at approximately the same value of  $A/Z$ . This can be compared to corresponding plots of efficiency against mass, see Figures 3a and 4a, where these peaks are located at  $A=13$  and  $A=11$  respectively.

## 5.8 Poor Fits in ROOT

The software ROOT was used in this project, not only to view and analyze data, but also to fit functions to histograms. To determine the efficiencies for the different simulations, the mass distribution was assumed to be a normal distribution. A program for ROOT was written in C++ to fit a Gaussian function to mass distribution histograms. The efficiency was calculated according to Equation 5, 6 and 7. The fits worked very well for most simulations, but not well for the simulations with few entries. Luckily, the simulations that resulted in very low efficiencies were not affected much by the bad fits as the integral and the number of tracked ions both were close to zero.

## 6 Conclusion

It can be concluded that the efficiency of the LAND/R<sup>3</sup>B-setup depends on several factors. Efficiencies of the setup vary in the range of 0 to 92 %. By changing the magnetic rigidity of ions, their beam-paths through ALADiN are changed, thereby giving them different directions, making them hit or miss detectors. Simulating nucleons being knocked out by adding momenta to the ions makes the beam wider, thus affecting the efficiency by making ions hit the detectors which had otherwise missed and vice versa.

The bending radius depends on the projectiles mass, charge and velocity for a constant magnetic field. Thus, these are the factors that influence where the beam hits the detectors. By varying these quantities we found that the detector that limits the detection of ions is the GFI2-detector. The beam can miss the detector on either side for sufficiently low or high magnetic rigidity.

While some answers regarding the questions about the LAND/R<sup>3</sup>B-setup are answered, partly or fully, in this report, there are still open questions left to investigate. For example, this project was limited to isotopes of carbon, boron and beryllium, which make up only part of the interesting ions studied in the LAND/R<sup>3</sup>B-setup.

# 7 Glossary

*4-momentum*, the four dimensional vector consisting of an energy component and the three dimensional momentum  $P = (E/c, \vec{p})$ .

$\chi^2$ -*test*, a method that associates weight functions to data points, here used to minimize the error when adapting a trajectory to the measured ion positions.

*Bandgap*, energy difference between bands.

*Bending radius*, the radius of the curvature of a deflection in a trajectory.

*Conduction band*, range of electronic states in which the electrons are free to move within the material.

*Entries*, here referring to the recorded particles.

*Evaporation of a nucleon*, the process where a nucleon gains enough energy to leave a nuclei.

*Impact parameter*, the perpendicular distance between the flight path of the projectile (here, ion) and the center of the target (here, target nuclei).

GEANT4, software used to simulate particle physics experiments.

GGLAND, a wrapper software for GEANT4.

*Kick*, addition of recoil momentum to an ion caused by the removal of a nucleon.

*Magnetic rigidity*, a measure of the effect a magnetic field has on the deflection of the trajectory of a particle.

*Monte Carlo method*, a class of stochastic simulation methods used for simulations.

ROOT, a CERN-developed software for data analysis.

*Scintillator*, a luminescent material (i.e. a material that can absorb the energy of incoming particles and thereafter emits it as radiation).

*Transverse momentum*, here referring to the component of the momentum of the ion that is perpendicular to the beam direction.

*Valence band*, range of electronic states of highest energy in which the electrons are still bound to nuclei.

# References

- [1] T. Aumann, "S393 Proposal - Neutron-rich Nuclei at and Beyond the Dripline in the Range  $Z=4$  to  $Z=10$  Studied in Kinematically Complete Measurements of Direct Reactions at Relativistic Energies", 2012; Tech report, 2012].
- [2] GSI, "Linearbeschleuniger UNILAC". Available: [https://www.gsi.de/forschung\\_beschleuniger/beschleunigeranlage/linearbeschleuniger.htm](https://www.gsi.de/forschung_beschleuniger/beschleunigeranlage/linearbeschleuniger.htm)(Accessed: 2016, May 11).
- [3] GSI, "Ringbeschleuniger SIS18 - der Rekordhalter". Available: [https://www.gsi.de/forschung\\_beschleuniger/beschleunigeranlage/ringbeschleuniger.htm](https://www.gsi.de/forschung_beschleuniger/beschleunigeranlage/ringbeschleuniger.htm)(Accessed: 2016, May 11).
- [4] A. Heinz, Private conversation, Gothenburg, May 2016.
- [5] GSI, "Experimental setup". Available: [https://www.gsi.de/work/forschung/nustarena/nustarena\\_divisions/kernreaktionen/research\\_program/reactions\\_with\\_exotic\\_nuclei/experimental\\_setup.htm](https://www.gsi.de/work/forschung/nustarena/nustarena_divisions/kernreaktionen/research_program/reactions_with_exotic_nuclei/experimental_setup.htm)(Accessed: 2016, May 11).
- [6] K. A. Olive and Particle Data Group, "Review of Particle Physics," Chinese Physics, vol 38, nr 9, 2014 Available: <http://pdg.lbl.gov/2015/download/rpp2014-Chin.Phys.C.38.090001.pdf>(Accessed: 2016, May 16).
- [7] W. R. Leo, "Techniques for Nuclear and Particle Physics Experiments"; Lausanne, 1987. Available: [http://tesla.phys.columbia.edu:8080/eka/William\\_R\\_Leo\\_Techniques\\_for\\_nuclear\\_and\\_partic.pdf](http://tesla.phys.columbia.edu:8080/eka/William_R_Leo_Techniques_for_nuclear_and_partic.pdf)(Accessed: 2016, May 16).
- [8] V. Panin, "Fully Exclusive Measurements of Quasi-Free Single-Nucleon Knockout Reactions in Inverse Kinematics"; Ph.D. thesis, Technische Universität Darmstadt, 2012.
- [9] National Nuclear Data Center, "Chart of Nuclides" [Online]. Available: <http://www.nndc.bnl.gov/chart/reCenter.jsp?z=4&n=4>(Accessed: 2016, May 11).
- [10] Geant 4, "Geant4 - a simulation toolkit", Website, CERN [Online]. Available: <http://www.sciencedirect.com/science/article/pii/S0168900203013688>(Accessed: 2016, April 18).
- [11] GGLAND, "GGLAND" [Online]. Available: <http://fy.chalmers.se/~f96hajo/ggland/>(Accessed: 2016, April 18).

[12] GGLAND, "The GGLAND command-line simulation wrapper" [Online]. Available: [http://fy.chalmers.se/~f96hajo/ggland/ggland\\_doc.pdf](http://fy.chalmers.se/~f96hajo/ggland/ggland_doc.pdf)(Accessed: 2016, April 18).

# A Tables of Efficiencies

## A.1 Reaction Products from a Beam of $^{16}\text{C}$

Table 2: Table of efficiencies from  $^{16}\text{C}$  in percent,  $\beta = 0.76$ , added momenta, kicks, are 400 MeV/c per nucleon. Entries marked with \* are from simulations of 1 000 000 events, otherwise 300 000 events are simulated.

Daughter Isotope	No Kick	One Nucleon	Two Nucleons	Three Nucleons
$^{15}\text{C}$	88.49	88.74	–	–
$^{14}\text{C}$	88.76	88.95	86.71	–
$^{13}\text{C}$	90.07	89.98	80.53	70.00
$^{12}\text{C}$	91.45	76.72	67.43	58.35
$^{11}\text{C}$	90.82	53.65	48.87	43.01
$^{10}\text{C}$	0.42	26.44	25.51	25.56
$^9\text{C}$	0.45	1.00	1.18	0.65
$^{15}\text{B}$	91.33*	77.08	–	–
$^{14}\text{B}$	90.34*	86.84	76.72	–
$^{13}\text{B}$	92.26*	89.29	79.81	69.49
$^{12}\text{B}$	88.06*	88.93	79.64	67.00
$^{11}\text{B}$	89.95*	89.43	72.04	60.17
$^{10}\text{B}$	91.25*	71.24	58.82	48.82
$^9\text{B}$	Unbound	–	–	–
$^8\text{B}$	0.86	19.77	18.88	18.55
$^{14}\text{Be}$	63.12*	47.94	47.11	–
$^{13}\text{Be}$	Unbound	–	–	–
$^{12}\text{Be}$	91.45*	70.05	62.47	54.20
$^{11}\text{Be}$	89.58*	79.86	66.40	55.87
$^{10}\text{Be}$	86.94*	87.89	64.69	53.43
$^9\text{Be}$	88.12*	86.26	57.40	47.08
$^8\text{Be}$	Unstable	–	–	–
$^7\text{Be}$	2.89	39.29	29.70	24.44

## A.2 Reaction Products from a Beam of $^{17}\text{C}$

Table 3: Table of efficiencies from  $^{17}\text{C}$  in percent,  $\beta = 0.74$ , added momenta, kicks, are 400 MeV/c per nucleon. Values are for simulations of 300 000 events each.

Daughter Isotope	No Kick	One Nucleon	Two Nucleons	Three Nucleons
$^{16}\text{C}$	88.37	88.41	–	–
$^{15}\text{C}$	88.69	88.86	87.31	–
$^{14}\text{C}$	90.07	89.53	81.65	70.66
$^{13}\text{C}$	91.47	81.75	70.66	60.91
$^{12}\text{C}$	91.42	60.94	55.09	48.29
$^{11}\text{C}$	0.38	36.44	33.52	32.01
$^{10}\text{C}$	0.26	7.21	14.18	15.48
$^9\text{C}$	0.19	0.33	3.03	5.29
$^{16}\text{B}$	Unbound	–	–	–
$^{15}\text{B}$	90.11	58.77	76.00	–
$^{14}\text{B}$	89.50	89.42	79.68	69.74
$^{13}\text{B}$	88.17	89.01	80.43	68.07
$^{12}\text{B}$	89.28	89.37	75.08	62.88
$^{11}\text{B}$	91.82	79.60	64.50	58.36
$^{10}\text{B}$	91.21	58.01	48.63	40.80
$^9\text{B}$	Unbound	–	–	–
$^8\text{B}$	0.41	4.19	11.44	12.15
$^{15}\text{Be}$	45.39	46.75	46.05	–
$^{14}\text{Be}$	91.48	57.51	54.98	46.75
$^{13}\text{Be}$	Unbound	–	–	–
$^{12}\text{Be}$	90.10	77.36	65.73	55.94
$^{11}\text{Be}$	88.12	86.43	66.56	55.09
$^{10}\text{Be}$	87.21	88.17	61.17	50.288
$^9\text{Be}$	90.43	75.47	52.36	42.08
$^8\text{Be}$	Unstable	–	–	–
$^7\text{Be}$	0.83	29.25	21.73	19.01

### A.3 Reaction Products from a Beam of $^{18}\text{C}$

Table 4: Table of efficiencies from  $^{18}\text{C}$  in percent,  $\beta = 0.72$ , added momenta, kicks, are 400 MeV/c per nucleon. Values are for simulations of 300 000 events each.

Daughter Isotope	No Kick	One Nucleon	Two Nucleons	Three Nucleons
$^{17}\text{C}$	89.61	89.61	–	–
$^{16}\text{C}$	88.67	89.06	87.69	–
$^{15}\text{C}$	90.05	89.97	83.70	73.03
$^{14}\text{C}$	91.34	86.34	74.34	64.45
$^{13}\text{C}$	91.47	66.60	59.79	51.31
$^{12}\text{C}$	45.13	44.69	40.44	36.38
$^{11}\text{C}$	0.72	0.45	0.47	0.46
$^{10}\text{C}$	0.61	1.67	0.88	0.56
$^9\text{C}$	1.71	1.52	1.60	5.40
$^{17}\text{B}$	91.78	76.45	–	–
$^{16}\text{B}$	Unbound	–	–	–
$^{15}\text{B}$	89.39	89.21	78.99	69.63
$^{14}\text{B}$	88.66	89.12	80.95	68.97
$^{13}\text{B}$	89.28	89.54	77.67	64.96
$^{12}\text{B}$	90.99	85.88	68.73	57.36
$^{11}\text{B}$	91.63	66.95	55.60	46.35
$^{10}\text{B}$	5.30	45.03	37.51	32.76
$^9\text{B}$	Unbound	–	–	–
$^8\text{B}$	0.00	0.07	0.09	0.04
$^{16}\text{Be}$	30.84	44.86	44.86	–
$^{15}\text{Be}$	91.13	55.69	53.68	48.08
$^{14}\text{Be}$	91.54	65.74	60.43	53.03
$^{13}\text{Be}$	Unbound	–	–	–
$^{12}\text{Be}$	89.07	83.63	66.97	56.00
$^{11}\text{Be}$	86.91	88.45	63.95	52.90
$^{10}\text{Be}$	89.07	84.42	56.74	46.31
$^9\text{Be}$	91.39	65.06	46.40	37.06
$^8\text{Be}$	Unstable	–	–	–
$^7\text{Be}$	0.55	18.93	15.58	14.23

# B Derivation of the Formula for the Magnetic Rigidity

This appendix aims to derive the expression for the magnetic rigidity,

$$B\rho = \frac{p}{q}, \quad (8)$$

where  $B$  is the magnetic field strength,  $\rho$  the bending radius,  $p$  the linear momentum magnitude and  $q$  the electric charge of a particle of mass  $m$ , moving in a circular path through a static magnetic field.

Such a particle will be affected by the Lorentz force,

$$\frac{d\vec{p}}{d\tau} = q\gamma(\vec{E} + \vec{v} \times \vec{B}). \quad (9)$$

Here  $\vec{v}$  is the velocity,  $\vec{p}$  the linear momentum  $\vec{p} = m\gamma\vec{v}$ ,  $\tau$  the proper time of the particle,  $c$  the speed of light,  $\gamma$  the Lorentz factor  $\gamma = (1 - \beta^2)^{-1/2}$ , where  $\beta = v/c$ . The electric field  $\vec{E}$  is zero in the case of the LAND/R<sup>3</sup>B-experiments. With  $dt/d\tau = \gamma$  we have

$$\frac{d\vec{p}}{dt} = q(\vec{v} \times \vec{B}). \quad (10)$$

Moving perpendicular to the magnetic field, the motion will be circular and the magnitude of the cross product  $\vec{v} \times \vec{B}$  is  $vB$ . For circular motion, the formula for gyro-frequency in cyclotrons can be used. First considering the nonrelativistic case, we have the centripetal force  $qvB = mv^2/\rho \Leftrightarrow \rho = mv^2/qvB$ . For a circular motion, the period,  $T$ , can be written as the path divided by the speed,  $T = 2\pi\rho/v = 2\pi m/qB$  which gives the angular frequency  $\omega = 2\pi/T = qB/m$ . In the relativistic case, mass must be corrected:  $\omega = qB/m\gamma$ . From this we have

$$\rho = \frac{v}{\omega} = \frac{\beta c}{\omega} = \frac{\gamma\beta cm}{qB} \Leftrightarrow B\rho = \frac{\gamma\beta cm}{q} = \frac{p}{q}, \quad (11)$$

which has been used in this project to calculate what velocities  $v = \beta c$  to use, in order to keep  $B\rho$  constant for different ions.

# C Positions of the Detectors in the Simulations

Table 5 shows the positions of the different detectors in the S393-experiment. Also, some additional data about the detectors is shown in the table.

Table 5: The positions of the detectors used in the simulations. The field gap for ALADiN has length = 175, width = 160 and height = 60.

Detector	Position [cm]	Rotation [degrees]
PSP	(0,0,-88.9)	-
POS	(0,0,-144.97)	-
SST1	(0,0,-6.44)	-
SST2	(0,0,-3.68)	-
SST3	(0,0,11.11)	-
SST4	(0.064,0.047,13.88)	ROTX=180
ALADiN center	(0,0,255)	-
GFI1	(-58.007,2.3,465.923)	ROTY=15
GFI2	(-73.969,0.0,525.461)	ROTY=15
TFW	(-229.506,-8.18,1121.307)	ROTY=15

# D C++ Function for Calculating Efficiencies

This script serves to determine the efficiency of a simulated isotope in LAND/R<sup>3</sup>B-setup. It fits a Gaussian function to the mass histogram and calculates the integral over an interval. Finally it calculates the efficiency by dividing that integral by the total number of simulated events.

```
1 double getEfficiency()
2 {
3     h102->Draw("fra_A>>hist2(10100,0,100)");
4     double first_bin = hist2->FindFirstBinAbove(0,1);
5     double last_bin = hist2->FindLastBinAbove(0,1);
6     double first_bin_pos = hist2->GetBinCenter(first_bin);
7     cout << "first_bin_pos =" << first_bin_pos << endl;
8     double last_bin_pos = hist2->GetBinCenter(last_bin);
9     cout << "last_bin_pos =" << last_bin_pos << endl;
10    h102->Draw("fra_A>>hist2(10100,0,100)");
11    double height = hist2->GetMaximum();
12    cout << "height =" << height << endl;
13    double mu = hist2->GetMean();
14    cout << "mu =" << mu << endl;
15    double sigma = hist2->GetRMS();
16    cout << "sigma =" << sigma << endl;
17    TF1 *myfit=new TF1("myfit","[0]*TMath::Exp(-((x-[1])^2)/(2*([2]^2)))"
18    ,mu-3 ,mu+3);
19    myfit->SetParameter(0,height);
20    myfit->SetParameter(1,mu);
21    myfit->SetParameter(2,sigma);
22    hist2->Fit(myfit,"R");
23    double limit_a = mu-4*sigma;
24    double limit_b = mu+4*sigma;
25    double A=myfit->Integral(limit_a,limit_b);
26    return (A*100)/300000;
27 }
```

# E Example of a GGLAND-script

This is a shell script for simulating 300 000 events of  $^{10}\text{B}$  with a velocity of  $0.74c$  through the LAND/R<sup>3</sup>B-setup from the target.

```
1 . geant4.sh;
2   /net/data1/sim2016/land022/scripts/ggland/land_geant4 \
3   --sst-3=z0=11.11cm \
4   --sst-4=rotx=180deg,x0=0.064cm,y0=0.047cm,z0=13.88cm \
5   --aladin=roty=-7deg,z0=255cm,I=-2500A \
6   --gfi-1=roty=-15deg,x0=-58.007cm,y0=2.3cm,z0=465.923cm \
7   --gfi-2=roty=-15deg,x0=-73.969cm,z0=525.461cm \
8   --tfw=roty=-15deg,x0=-229.506cm,y0=-8.18cm,z0=1121.307cm,\
9   paddle_spacing1=0cm,paddle_spacing2=0cm,\
10  paddle_width1=10.188889cm,paddle_width2=10.185714cm \
11  --gun=beta=0.74,setboost,feed=A,dummy \
12  --gun=from=A:1,B10,box,sx=1cm,sy=1cm,sz=0.01cm,p=400MeV/c,\
13  isotropic,boost \
14  --tree=land02track,allevents,part,nonreduced,/net/data1/
15  sim2016/sim/C17/B10/B101k400.root \
16  --np \
17  --events=300000;
```

# F Förkortad version på svenska

Här följer en sammanfattad version av rapporten på svenska. Sammanfattningen avser att beskriva det mest väsentliga i rapporten.

## F.1 Inledning

De lättaste grundämnena skapades en kort tid efter universums födelse. Därefter ansamlades materia och bildade stjärnor i vilka grundämnen som beryllium kunde skapas för första gången. Vetenskapens önskan att förstå processerna i nukleosyntes är ett av de främsta skälen att studera kärnreaktioner. Detta är en av anledningarna att kärnreaktioner studeras i partikelaccelerationer över hela världen. Av praktiska skäl är instabila kärnor inte lika välstuderade som stabila. Först sedan 80-talet finns anläggningar som kan producera radioaktiva kärnor. Många kärnfysikexperiment fokuserar därför speciellt på instabila kärnor.

År 2010 utfördes ett experiment på lätta, instabila, neutronrika kärnor (S393-experimentet) på Gesellschaft für Schwerionenforschung (GSI) i Darmstadt, Tyskland. Experimentet använde LAND/R<sup>3</sup>B-uppställningen för att mäta 4-vektorerna hos joner och partiklar, med hjälp av detektorer av olika slag. När resultaten från experimentet i LAND/R<sup>3</sup>B-uppställningen ska analyseras är det viktigt att veta detektionsbegränsningarna, det vill säga under vilka förutsättningar reaktionsprodukterna inte kan detekteras. Det är av intresse att undersöka såväl antalet fragment som missar detektorerna, eller förloras på vägen genom experimentuppställningen, som antalet fragment som rekonstrueras felaktigt<sup>3</sup>.

Avsikten med detta projekt är att finna detektionsbegränsningarna i LAND/R<sup>3</sup>B-uppställningen. Uppställningen har använts i flertalet experiment, bland annat S393-experimentet, och kommer också användas i framtida experiment. Detektionsbegränsningarna ska undersökas genom simuleringar med programmet GEANT4 tillsammans med GGLAND, samt analysprogrammet LAND/R<sup>3</sup>B-TRACKER. Att använda just dessa program är en viktig del av uppgiften eftersom samma mjukvara används vid analys av experiment med LAND/R<sup>3</sup>B-uppställningen. Detektionsbegränsningarna kommer undersökas genom att mäta effektiviteten av rekonstruktionen. Denna definieras som kvoten mellan antalet korrekt rekonstruerade händelser och det totala antalet simulerade händelser. Effektiviteten kommer att mätas för olika isotoper och med adderad transversell rörelsemängd för att se hur dessa parametrar påverkar rekonstruktionen. Den transversella rörelsemängd ett fragment har i experimentuppställ-

---

<sup>3</sup>Med rekonstruktion menas användandet av data från detektorerna i fysikaliska lagar för härledning av massstalsvärden och 4-vektorer av rörelsemängd.

ningen kommer att påverka dess bana och på så vis göra att den träffar detektorerna på andra positioner.

## F.2 Bakgrund

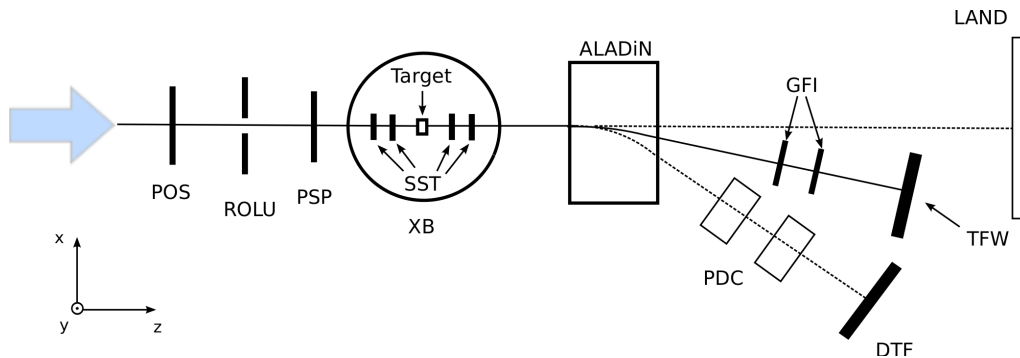
I detta avsnitt behandlas teorin som behövs för att förstå projektet. Nedanstående stycken beskriver experimentuppställningen och tre av dess detektorer, samt de ekvationer som används för att identifiera fragmenten.

### F.2.1 LAND/R<sup>3</sup>B-uppställningen och S393-experimentet

Detta projekt analyserar experimentuppställningen LAND/R<sup>3</sup>B. Ett experiment som utförts med denna uppställning var S393-experimentet. Experimentet fokuserar på neutronrika kärnor med atomnummer 4 till 10. Som kan läsas i experimentansökan [1], är de två största motiven bakom experimentet att förstå reaktionsförhållandena bakom astrofysikaliska nukleosyntesprocesser samt att undersöka kärnstrukturer nära gränsen för bundna kärnor.

Experiment med LAND/R<sup>3</sup>B-uppställningen studerar instabila kärnor med halveringstider i storleksordningar ner till millisekunder. Så kortlivade kärnor måste produceras på plats. För att göra detta används en linjär partikelaccelerator (UNILAC), en synkrotron (SIS18) och en fragmentseparator (FRS). I UNILAC och SIS18 får joner en hög hastighet, upp till 90 procent av ljushastigheten. Därefter kolliderar de med ett relativt lätt mål, varpå jonerna fragmenteras. Fragmenten går sedan genom FRS som sorterar ut de isotoper som är av intresse.

Efter FRS leds jonerna till experimentuppställningen LAND/R<sup>3</sup>B. Där kolliderar strålen av joner med ett stationärt mål som kan vara av kol, bly eller plast. Reaktionsprodukterna separeras sedan i termer av magnetisk rigiditet genom användning av en stor magnet (ALADiN), innan de går igenom detektorer av olika typer. Experimentuppställningen illustreras i Figur 13.



Figur 13: Skiss av LAND/R<sup>3</sup>B-uppställningen vilken användes i S393-experimentet. Den breda pilen motsvarar den inkommande jonstrålen. Jonerna som kolliderar med kärnorna i målet fragmenteras. Reaktionsprodukterna separeras och detekteras i neutron-, fragment- respektive protonarmarna.

## F.2.2 Introduktion av de tre mest relevanta detektorerna

Tre detektorer som är av speciellt intresse för projektet är SST, GFI respektive TFW, se också Figur 13. Två SST-detektorer finns placerade efter målet i strålriktningen. Dessa mäter energiförlust samt position för de utgående jonerna. Principen för metoden är att jonerna exciterar elektroner i det halvledande detektormaterialet. Genom att lägga en elektrisk spänning över detektorerna kan man mäta strömpulsarna av dessa exciterade elektroner.

Efter ALADiN finns två GFI-detektorer som mäter den horisontella positionen hos joner. Dessa består av scintillatorer. Scintillatorer är material med förmågan att absorbera energin från passerande partiklar och utsända detta i form av ljus.

TFW-detektorn mäter position, energiskillnad och tid i LAND/R<sup>3</sup>B-uppställningen. Den består av två plan av scintillatorer som är placerade både vertikalt och horisontellt och ger då information om de ingående jonernas position i båda riktningar.

## F.2.3 Rekonstruktion av jonerna

Storheter som massa och rörelsemängd hos jonerna kan rekonstrueras med datan som fås från detektorerna i LAND/R<sup>3</sup>B-uppställningen. Krökningen av respektive jons bana genom magnetfältet i ALADiN kan rekonstrueras från de positioner som bestämts av detektorerna. Genom en relativistisk behandling av ekvationen för Lorentzkraften tillsammans med ekvationen för cirkulär rörelse kan följande samband härledas, se Appendix B,

$$B\rho = \frac{\gamma\beta cm}{q} \propto \frac{A}{Z}, \quad (12)$$

där  $B\rho$  är den magnetiska rigiditeten hos den inkommande jonen,  $\gamma$  är Lorentzfaktorn,  $m$  är jonmassan och  $q$  är jonens elektriska laddning. Jonens hastighet är  $v = \beta c$ , där  $c$  är ljushastigheten. Jonmassan är proportionell mot jonens masstal,

A. Om jonerna är fullständigt joniserade, som de är i LAND/R<sup>3</sup>B-experimenten, är deras elektriska laddning proportionell mot deras atomnummer  $Z$ .

Enligt Bethe-Blochekvationen, Ekvation 3, är jonernas energiförlust i SST- och TFW-detektorerna proportionell mot kvadraten av atomnumret för jonen. Genom att mäta energiförlusten kan således jonernas atomnummer rekonstrueras och sättas in i Ekvation 12, varpå masstalet och rörelsemängden kan fås.

## F.2.4 Resultat av kollisionerna

Kollisionerna mellan jonerna och målet kan slå ut olika antal nukleoner från kärnan. Reaktionerna som sker vid kollisionerna varierar. I vissa fall kan reaktionen mellan jonen och en fri nukleon i målet approximeras till en reaktion mellan två nukleoner, och i andra fall inte. Energi- och rörelsemängdskonservering medför att jonen utsätts för en rekyl när nukleoner slås ut. Storleken av denna rekyl beror på rörelsemängden hos den borttagna nukleonen. 2011 publicerades en doktorsavhandling av Panin [8], i vilken rörelsemängden hos protoner i en <sup>12</sup>C-kärna undersöktes. Panins resultat har använts i detta projektet för att uppskatta en realistisk storlek hos den ovan nämnda rekylen.

Efter kollisionen kan jonerna vara exciterade. Detta kan göra att de förlorar en eller flera nukleoner för att återgå till ett stabilt energitillstånd. Det innebär att ett stort antal reaktionsprodukter kan förekomma och därför måste simuleras. Av de möjliga dotterkärnorna som behandlas i detta projektet är <sup>8</sup>Be, <sup>13</sup>Be, <sup>9</sup>B och <sup>16</sup>B obundna eller med halveringstider betydligt lägre än den typiska tiden som joner färdas i LAND/R<sup>3</sup>B-uppställningen. Möjligheten att detektera dessa isotoper kan därför försummas och simuleringar för <sup>8</sup>Be, <sup>13</sup>Be, <sup>9</sup>B och <sup>16</sup>B kommer inte att göras.

## F.3 Simuleringar

För att hitta detektionseffektiviteten för LAND/R<sup>3</sup>B-uppställningen och S393-experimentet har simuleringar använts. Simuleringar är ett viktigt verktyg i analys av experiment. I simuleringar är det möjligt att definiera såväl inparametrar som detektorupplösning vilket möjliggör isolerade undersökningar av skilda parametrar. De viktigaste programmen i detta projekt har varit GGLAND, GEANT4 och LAND/R<sup>3</sup>B-TRACKER. Dessa beskrivs nedan tillsammans med simulerings- och analysprocesserna.

### F.3.1 Mjukvara

GEANT4 är ett verktyg för att simulera högenergipartikelexperiment. Det utgår från en *physics list* som definierar fysikaliska modeller och faktorer. Den *physics list* som användes i detta projektet var QGSP\_BERT. Metoden som används av GEANT4 är en Monte Carlo-metod, en stokastisk metod som använder slumpantal.

GGLAND är ett kommandoradbaserat wrapper-program för GEANT4. GGLAND tillhandahåller användaren med *.root*-filer efter körning [10].

LAND/R<sup>3</sup>B-TRACKER är ett program som rekonstruerar jonernas bana genom experimentuppställningen. Detta görs baserat på data från detektorerna och genom minimering av ett  $\chi^2$ -test. Ett  $\chi^2$ -test är en metod för att mäta felet mellan simulerad eller experimentell data och teoretisk data. LAND/R<sup>3</sup>B-TRACKER använder information från *.root*-filen från GGLAND.

### F.3.2 Realistisk rekyl

För att få simuleringarna att efterlikna experimentet är det viktigt att bestämma en realistisk rekyl. För att göra detta har resultatet från Panins doktorsavhandling "Fully Exclusive Measurements of Quasi-Free Single Nucleon Knockout Reactions in Inverse Kinematics" [8] använts. Dessa mätningar innehåller de inre rörelsemängderna för protoner i p- och s-orbitaler. Det visar sig att protoner i p- och s-orbitaler har som mest ungefär 350 MeV/c respektive 400 MeV/c rörelsemängd. I detta projektet används approximationen att neutroner i p- och s-orbitaler har samma rörelsemängder som respektive protoner.

Som kan ses i formeln för relativistisk hastighetsaddition, Ekvation 4, är rörelsemängden densamma i nukleonens referenssystem i fallet då rekylen sker i transversell riktning relativt jonstrålen. Värdet 400 MeV/c har därför använts som maximal transversell rekyl från borttagning av en nukleon.

### F.3.3 Simuleringsmetod och dataanalys

Simuleringarna utfördes i GGLAND som är ett wrapperprogram till GEANT4. Jonkanon, som genererar den inkommande strålen, och detektorerna placeras i en simulerad volym genom att definiera position och rotation. Tabellen Appendix C innehåller exakta positioner för alla detektorer. Jonkanonen är formad som en kvadrat för att efterlikna målet i experimentet. Hastigheten på jonerna varierar mellan 72 och 76 procent av ljushastigheten. Rekylen för varje jon introduceras genom addition av 400 MeV/c per borttagen nukleon i en slumpmässig riktning i jonens vilosystem. För att efterlikna en detektorupplösning som inte är perfekt adderas ett slumptal från en normalfördelning till utdatan. Resultaten i rapporten innehåller antingen 300 000 eller 1 000 000 simulerade joner.

För att analysera simulerad data som lagras i *.root*-filer används ROOT, ett dataanalysprogram utvecklat på CERN. Datan sorteras och studeras i histogram, bland annat för träffpositioner på detektorerna. Genom att titta på träffpositioner har slutsatser om var effektivitet går förlorad kunnat dras.

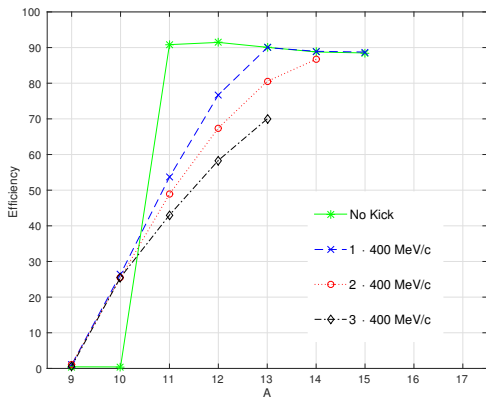
För att fastställa effektiviteten antas de rekonstruerade masstalen från simuleringarna vara normalfördelade. För att bestämma andelen korrekt rekonstruerade masstal görs en anpassning av en Gaussfunktion till masstalshistogrammet. Integralen över denna anpassningen, från medelvärdet plus/minus fyra standardavvikelser, antas vara korrekta händelser. Effektiviteten är kvoten av antalet korrekt rekonstruera-

de masstal och det totala antalet simulerade joner. Rekonstruktionseffektiviteterna presenteras i figurer i nästa stycke och i tabeller i Appendix A.

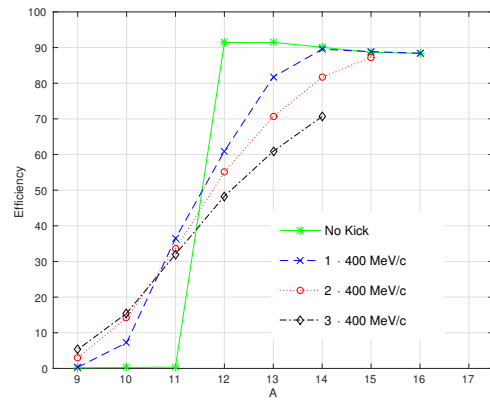
## F.4 Resultat

Mätningarna i detta projekt resulterade i nio mätserier av effektiviteten. Tre kolsotoper,  $^{16}\text{C}$ ,  $^{17}\text{C}$  och  $^{18}\text{C}$  valdes med motsvarande  $\beta$  så att  $B\rho$  hölls konstant. För var och en av de tre isotoperna simulerades fragment av kol, bor och beryllium. För varje fragment gjordes simuleringar utan tillagd rörelsemängd och med tillagd rörelsemängd från en, två eller tre utslagna nukleoner, som var och en bidrog med 400 MeV/c rörelsemängd i en slumpvald riktning.

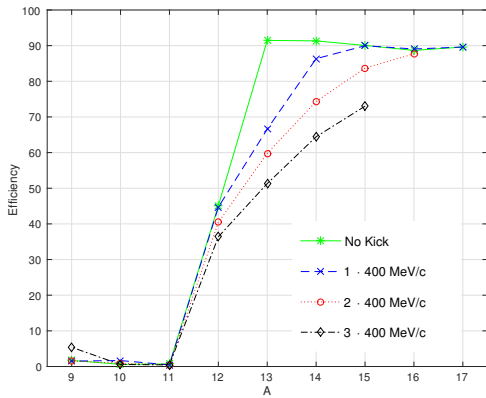
För kol var effektiviteten nästan konstant runt 90 % för de joner utan adderad rörelsemängd, för att sedan sjunka drastiskt för lägre massor. För de joner som adderats rörelsemängd var denna nedgång mer gradvis, vilket kan ses i Figurer 14a, 14b och 14c. Detta kan förklaras med att strålens träffyta på detektorerna förstöras av tillagd rörelsemängd. För bor uppvisas ett liknande mönster men här kan tilläggas att de joner som fått tillagt rörelsemängd från en eller två nukleoner har minskande effektivitet för simuleringar med höga massor. Detta kan förklaras med att strålen även missar på andra sidan av detektorerna. Detta illustreras i Figurer 14d, 14e och 14f. För beryllium kan observeras att även de joner som inte tillagts någon extra rörelsemängd visar sig missa detektorerna på båda sidor. Detta inses genom att studera de konkava graferna i Figurer 14g, 14h och 14i som visar på att strålen missar detektorer på ena sidan för låga massor och på andra sidan för höga.



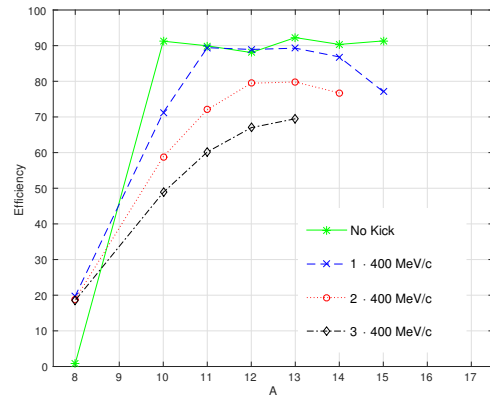
(a) Effektiviteter för koljoner som producerats i en reaktion med en stråle av  $^{16}\text{C}$ .



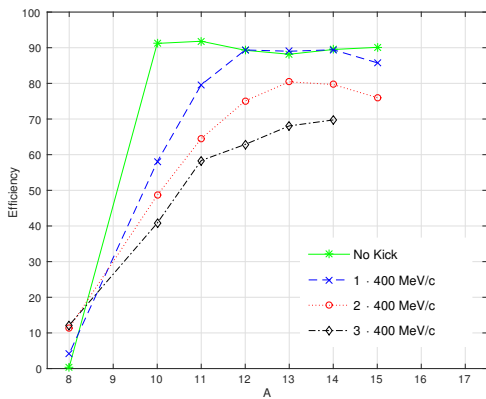
(b) Effektiviteter för koljoner som producerats i en reaktion med en stråle av  $^{17}\text{C}$ .



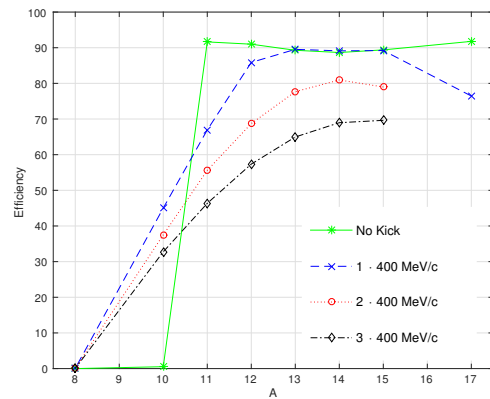
(c) Effektiviteter för koljoner som producerats i en reaktion med en stråle av  $^{18}\text{C}$ .



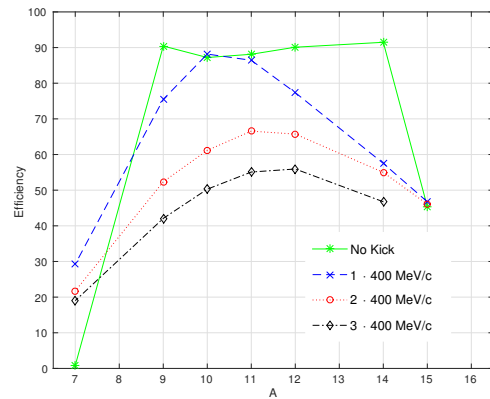
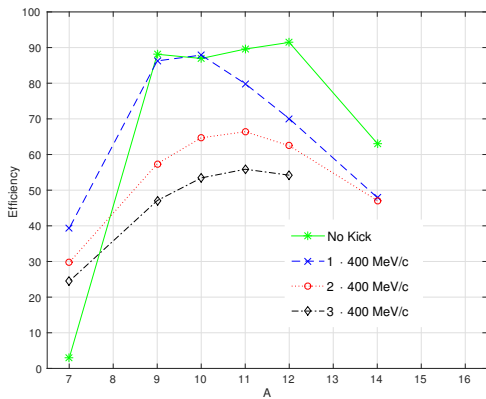
(d) Effektiviteter för borjoner som producerats i en reaktion med en stråle av  $^{16}\text{C}$ .



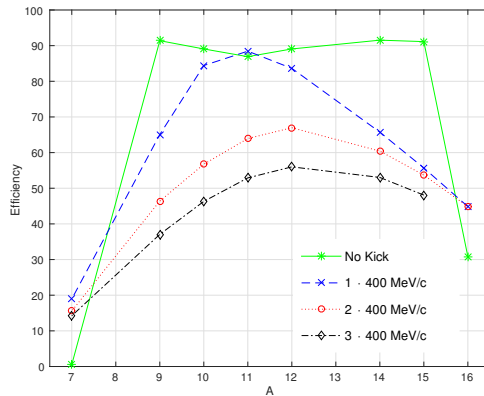
(e) Effektiviteter för borjoner som producerats i en reaktion med en stråle av  $^{17}\text{C}$ .



(f) Effektiviteter för borjoner som producerats i en reaktion med en stråle av  $^{18}\text{C}$ .



(g) Effektiviteter för berylliumjoner som producerats i en reaktion med en stråle av  $^{16}\text{C}$ . (h) Effektiviteter för berylliumjoner som producerats i en reaktion med en stråle av  $^{17}\text{C}$ .



(i) Effektiviteter för berylliumjoner som producerats i en reaktion med en stråle av  $^{18}\text{C}$ .

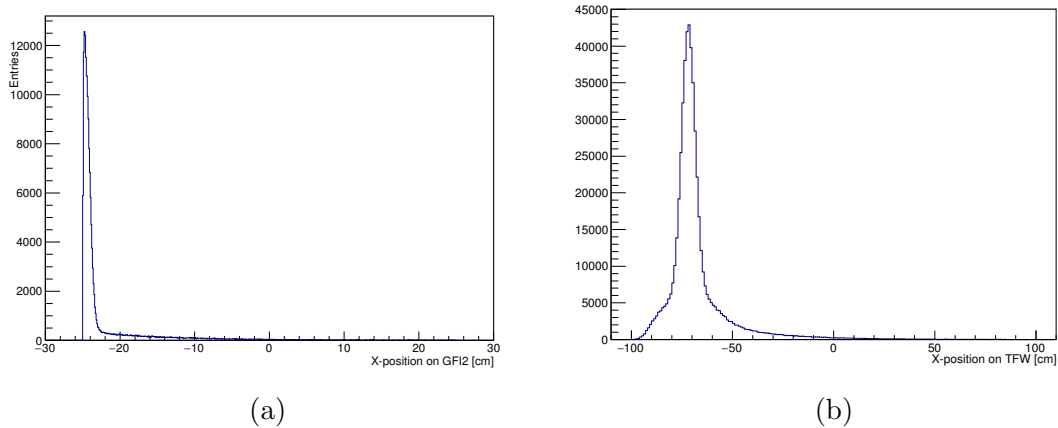
Figur 14: Effektiviteter för olika joner, producerade i olika reaktioner av olika isotoper och med olika mycket rekyl från utslagna nukleoner. De flesta joner visar sjunkande effektivitet för låga massor, och somliga, särskilt beryllium visar även på lägre effektivitet för höga massor. Den maximala effektiviteten tycks ligga på runt 90 %. De joner med tillagd rörelsemängd sjunker mer gradvis i effektivitet än de utan som är mer skarpa.

## F.5 Diskussion

I detta stycket diskuteras flera ämnen, däribland den maximala effektiviteten, effekten av att ta bort nukleoner, vilka detektorer som träffas och missas, hur kicken påverkar effektiviteten, strålens storlek, samt hur strålen är kopplad till den magnetiska rigiditeten. Vissa felkällor som kan tänkas ha påverkat resultaten av detta projekt diskuteras också.

### F.5.1 Begränsande detektorer och maximal effektivitet

En viktig frågeställning är vilken detektor som begränsar effektiviteten. I Figur 5a visas de registrerade  $x$ -koordinaterna vid GFI2-detektorn för rekonstruerade fragment av  $^{12}\text{C}$  utan kick. En skarp minskning vid vänstersidan av histogrammet kan ses, vilket indikerar att jonstrålen delvis skärs av vid kanten av GFI2-detektorn. Figur 5b visar samma data från samma simulering vid TFW-detektorn och här ses inte någon liknande minskning av effektiviteten. Detta indikerar att hela strålen träffar TFW. GFI1 ger liknande resultat som TFW och den begränsande detektorn verkar därför vara GFI2.



Figur 15: Histogram som visar de registrerade  $x$ -positionerna i GFI2 (a) och TFW (b) för simulerade  $^{12}\text{C}$ -joner med moderjon  $^{17}\text{C}$ .

### F.5.2 Den maximala effektiviteten

Den maximala effektiviteten som uppmättes i våra simuleringar var cirka 90 %, detta ses främst för joner utan rekyl men även för joner med rekyl från en nukleon. Det noteras för joner utan rekyl att detektorerna registrerar fler händelser när man rör sig i strålriktningen. Det visar att strålen reagerar med luft samt tidigare detektorer vilket producerar produkter som registreras av efterföljande detektorer. Dessa reaktioner kan deflektera de simulerade jonerna så att de missar efterföljande detektorer eller försvårar rekonstruktionen av dem. Det minskar den maximala effektiviteten.

När LAND/ $\text{R}^3\text{B}$ -TRACKER försöker beräkna flygbanor för fragment försöker den göra en anpassning där  $\chi^2$  minimeras. LAND/ $\text{R}^3\text{B}$ -TRACKER klarar ibland inte av att hitta en flygbana som passar datan från detektorerna. Detta leder till att  $\chi^2$  och residualerna för de olika detektorerna blir stora. Man ser att när LAND/ $\text{R}^3\text{B}$ -TRACKER hittar en anpassning där fragmentmassan skiljer sig mycket från den simulerade massan så leder det till höga värden för  $\chi^2$  och residualer.

### F.5.3 Påverkan av rekyl

Joner som inte utsätts för en rekyl kommer att skapa en fokuserad stråle, som upplever endast en låg spridning. Rekyl från utslagna nukleoner kommer leda till att

strålen breddas, vilket leder till att det skapas en större träffyta på detektorerna. Det kan leda till att delar av den hamnar utanför detektorerna. Detta leder generellt till att effektiviteten minskar när rekylen ökar.

Det förekommer fall då effektiviteten ökar med rekyl. Dessa fall uppkommer då strålen, som består av jonerna som inte utsatts för rekyl, missar en detektor, medan den ökade strålbredden med rekyl ser till att en del av strålen träffar detektorn igen.

## F.6 Slutsats

Det har visats att detektionseffektiviteten i LAND/R<sup>3</sup>B-uppställningen beror på ett flertal faktorer. Effektiviteterna i uppställningen varierar mellan värden på 0 till cirka 92 %. Ändring av den magnetiska rigiditeten hos jonerna påverkar deras banor genom ALADiN och på så vis hur de träffar detektorerna. Simuleringar med extra transversell rörelsemängd, som motsvarar rekyl från reaktioner, gör strålen bredare och påverkar på så vis effektiviteten då jonerna som annars träffat detektorerna kan missa och vice versa.

Avböjningen av jonernas banor beror på jonernas massa, laddning och hastighet i ett konstant magnetfält. Därför är det dessa faktorer som påverkar var detektorerna träffas. Variation av dessa faktorer har visat att den begränsande detektorn är GFI2.